

FINAL REPORT

Inversion of High Frequency Acoustic Data for Sediment
Properties Needed for the Detection and Classification of UXOs

SERDP Project MR-2229

MAY 2015

Brian T. Hefner
University of Washington

Distribution Statement A

This document has been cleared for public release



This report was prepared under contract to the Department of Defense Strategic Environmental Research and Development Program (SERDP). The publication of this report does not indicate endorsement by the Department of Defense, nor should the contents be construed as reflecting the official policy or position of the Department of Defense. Reference herein to any specific commercial product, process, or service by trade name, trademark, manufacturer, or otherwise, does not necessarily constitute or imply its endorsement, recommendation, or favoring by the Department of Defense.

REPORT DOCUMENTATION PAGE

*Form Approved
OMB No. 0704-0188*

The public reporting burden for this collection of information is estimated to average 1 hour per response, including the time for reviewing instructions, searching existing data sources, gathering and maintaining the data needed, and completing and reviewing the collection of information. Send comments regarding this burden estimate or any other aspect of this collection of information, including suggestions for reducing the burden, to Department of Defense, Washington Headquarters Services, Directorate for Information Operations and Reports (0704-0188), 1215 Jefferson Davis Highway, Suite 1204, Arlington, VA 22202-4302. Respondents should be aware that notwithstanding any other provision of law, no person shall be subject to any penalty for failing to comply with a collection of information if it does not display a currently valid OMB control number.

PLEASE DO NOT RETURN YOUR FORM TO THE ABOVE ADDRESS.

1. REPORT DATE (DD-MM-YYYY)	2. REPORT TYPE	3. DATES COVERED (From - To)
------------------------------------	-----------------------	-------------------------------------

4. TITLE AND SUBTITLE	5a. CONTRACT NUMBER
	5b. GRANT NUMBER
	5c. PROGRAM ELEMENT NUMBER

6. AUTHOR(S)	5d. PROJECT NUMBER
	5e. TASK NUMBER
	5f. WORK UNIT NUMBER

7. PERFORMING ORGANIZATION NAME(S) AND ADDRESS(ES)	8. PERFORMING ORGANIZATION REPORT NUMBER
---	---

9. SPONSORING/MONITORING AGENCY NAME(S) AND ADDRESS(ES)	10. SPONSOR/MONITOR'S ACRONYM(S)
	11. SPONSOR/MONITOR'S REPORT NUMBER(S)

12. DISTRIBUTION/AVAILABILITY STATEMENT

13. SUPPLEMENTARY NOTES

14. ABSTRACT

15. SUBJECT TERMS

16. SECURITY CLASSIFICATION OF:			17. LIMITATION OF ABSTRACT	18. NUMBER OF PAGES	19a. NAME OF RESPONSIBLE PERSON
a. REPORT	b. ABSTRACT	c. THIS PAGE			19b. TELEPHONE NUMBER (Include area code)

Table of Contents

Table of Contents.....	i
List of Tables.....	ii
List of Figures.....	ii
List of Acronyms	iv
Keywords.....	iv
Acknowledgements	iv
Abstract.....	1
Objectives.....	1
Technical Approach	1
Results	2
Benefits.....	2
Objective	3
Background	4
Materials and Methods.....	5
Teledyne-RESON Seabat 7125	5
Environmental Characterization.....	6
<i>In-situ Measurement of Porosity 2 (IMP2)</i>	6
<i>Seafloor Laser Scanner (SLS)</i>	7
<i>Sediment Sampling</i>	7
<i>“Attenuation Array” and InSEA</i>	8
Inversion of MBES data.....	9
<i>Preprocessing</i>	9
<i>First Stage</i>	12
<i>Second Stage</i>	13
<i>Third Stage</i>	15
<i>Data vector</i>	15
<i>Additional outputs</i>	15
Results and Discussion	17
Gulf Experiment 2011 (GulfEx11).....	17
Target and Reverberation Experiment 2013 (TRES13).....	21
<i>MBES Data</i>	22
<i>Environmental Data</i>	23
<i>Inversion Results And Comparisons With Measured Predictions</i>	28
St. Andrew’s Bay Experiment 2014 (BayEx14)	34
<i>MBES Data</i>	34
<i>Environmental Data</i>	35
<i>Inversion Results and Comparisons With Measured Parameters</i>	37
Conclusions and Implications for Future Research/Implementation.....	44
Literature Cited.....	47

List of Tables

Table 1: Environmental measurements and locations at along the MBES track.....	24
Table 2: Density and porosity determined from diver cores collected along the multibeam track.....	26
Table 3: Spectral strengths and exponents for the BayEx14 sediment interfaces.	35
Table 4: Spectral strengths and exponents for the density fluctuation power spectra within the sand sediment.....	37

List of Figures

Figure 1: Teledyne-RESON Seabat 7125.....	5
Figure 2: The IMP2 (left image) and the SLS (right image).	6
Figure 3: The "attenuation array" (left image) and the InSEA (right image).	8
Figure 4: Inversion algorithm flow chart.....	10
Figure 5: Linear fit to the bathymetric return in the beamformed MBES data. This linear fit determines the effective roll of the ship relative to the seafloor.	11
Figure 6: Example of model time series for interface (red) and volume (blue) scattering, 250 kHz, 8.5° off-nadir.	13
Figure 7: Example of fit of small-slope model to interface scattering strength obtained from inversion. This is the sand section of the TREX13 track; the frequency is 300 kHz.....	14
Figure 8: (a) IMP2/SLS being deployed during GulfEx11. (b) Example of a seafloor DEM measured during GulfEx11 with the laser line intensity superimposed to distinguish between shells and sand. (c) Complete DEM measured during a single SLS deployment at the experiment site.	18
Figure 9: (a) Scattering strengths at normal incidence determined from the inversion (black lines) and the environmental characterization (red lines). In both cases, the interface scattering strengths are shown as the dot-dashed lines and the volume scattering contribution is shown as the dashed lines. (b) Scattering as a function of grazing angle for each frequency.....	18
Figure 10: (a) Roughness power spectra determined from the DEM shown in Figure 8(c). The red line is a power law fit to the roughness spectra used to determine the two-dimensional power-law spectral fit, the parameters of which are shown. (b) The shell size distribution measured at the GulfEx11 site (red and blue circles) compared to the sand and shell distribution measured during SAX04.....	20
Figure 11: IMP2 and SLS late in GulfEx11.....	20
Figure 12: Attenuation at the GulfEx11 site found from an inversion of the multibeam data.....	21
Figure 13: Bathymetry and distribution of assets for main reverberation component of TREX13. The location of the MBES Study Site to support the multibeam inversion work indicated to the southeast of the R/V Sharp.....	22

Figure 14: (a) Backscatter measured using the multibeam sonar during the survey cruise at the start of TREX13. The multibeam measurement track is shown as the red line. (b) The scattering strength (upper panel) and bathymetry (lower panel) along the inversion line..... 22

Figure 15: Pole mount used deploy the Seabat 7125 sonars from the R/V Sharp during TREX13. 23

Figure 16: Locations of the environmental measurements along the MBES track. 24

Figure 17: 1D roughness power spectra measured along the MBES measurement track. 25

Figure 18: (a) Spectral exponent and (b) spectral strength determined from a power law fit to the roughness power spectra measured along the MBES measurement track. (c) Roughness power spectra and the spectral fits for sites #1 and #8. 26

Figure 19: Shell weight distribution (Upper panel) and shell number density (lower panel) for site #1 (blue), site #4 (red), and site #8 (black). 27

Figure 20: Sound speed (upper panel) and loss parameter or wavenumber ratio (lower panel) measured using the InSEA along the multibeam track. 27

Figure 21: Map of the density ratio along the TREX13 track determined from the MBES inversion. The background is the scattering strength measured by de Moustier and Kraft during the experiment. 29

Figure 22: Volume scattering strength along the TREX13 track (blue) compared to model predictions made using the measured sediment properties and shell distributions (red). 30

Figure 23: Volume scattering strength measured at 0 m, 150 m, and 350 m along the TREX13 track (blue) compared to ground truth predictions (red). 30

Figure 24: Loss Parameter determined from stage 1 of the inversion, from the inversion *IOI* result, and the InSEA. 32

Figure 25: Roughness Spectra along the TREX13 track compared to the spectra measured using the SLS. Each panel corresponds to a different wavenumber. 32

Figure 26: Sound Speed Ratio (upper), Porosity (middle), and Density Ratio (lower) determined using the inverted *IOI* (blue points). The measured values are also shown (red points). 33

Figure 27: Configuration of the R/V Sharp and mooring lines relative to the MBES track The inset shows the mooring location relative to the shoreline along the bay. 34

Figure 28: (Left panel) Formation factor measured using the IMP2 at the BayEx14 site. (Right panel) The mean spectra for the mud/water and sand/mud interfaces extracted from the formation factor data. 35

Figure 29: Density fluctuation power spectra within the underlying sand sediment. 36

Figure 30: Sound speed ratio and Attenuation measured in the mud layer (left panels) and the underlying sand (right panel). 36

Figure 31: The inversion volume scattering strength along the BayEx14 track (blue) compared to scattering strength determined from the measured density fluctuations (red) in the sand sediment. 38

Figure 32: Inverted volume scattering strength (blue) at the 100 m distance along the BayEx14 track compared to the scattering predictions (red). 38

Figure 33: Results of a modified inversion which treats the top 15 cm of the half-space as a layer with different point volume scatterers from those scatterers below the layer. 39

Figure 34: Loss Parameter determined from stage 1 of the inversion, from the inversion *IOI* result, and the attenuation array. 41

Figure 35: Roughness Spectra along the BayEx14 track compared to the spectra measured using the SLS. Each panel corresponds to a different wavenumber. 41

Figure 36: Sound Speed Ratio (upper), Porosity (middle), and Density Ratio (lower) for BayEx14 determined using the *IOI* determined from the inversion. The measured values are also shown..... 42

List of Acronyms

PC SWAT	Personal Computer Shallow Water Acoustic Toolset
UXO	Unexploded Ordnance
MBES	Multibeam Echo Sounder
GulfEx11	Gulf Experiment 2011
TREX13	Target and Reverberation Experiment 2013
BayEx14	Bay Experiment 2014
APL-UW	Applied Physics Laboratory, University of Washington
MSE	Mean-square-error
SAX99	Sediment Acoustics Experiment 1999
SAX04	Sediment Acoustics Experiment 2004
IMP2	In-Situ Measurement of Porosity 2
SLS	Seafloor Laser Scanner
STMS1	Sediment Transmission Measurement System 1
InSEA	Investigation of Sediments by Acoustics
SS	Small Slope
DEM	Digital Elevation Map
IOI	Index of Impedance

Keywords

underwater munitions, acoustic response, UXO detection and characterization, high frequency acoustic data inversion

Acknowledgements

This project benefited greatly from SERDP and ONR-funded experiments in 2011, 2013, and 2014 and the PIs involved in those efforts: Drs. Steve Kargl, Kevin Williams, Aubrey Espana, DJ Tang, and Jie Yang. Many thanks to Teledyne-RESON and in particular Drs. Gorm Wendelboe and Eric Maillard, who provided the Seabat 7125s used in this project as well as technical assistance.

Abstract

Objectives

An essential component in the detection and characterization of underwater munitions is knowledge of the acoustic response of the environment as well as the environment's effect on the acoustic response of munitions. Simulation tools and technologies have been developed under SERDP-funded research initiatives, such as the Personal Computer Shallow Water Acoustic Toolset (PC SWAT), to model the acoustics of both the environment and the munitions. The evaluation of these technologies, as well as their future use in unexploded ordnance (UXO) remediation, rely on knowledge of the underwater environment, particularly the properties of the seafloor. Conventional methods for determining relevant seabed properties employ time-consuming point measurements. Commercially available high-frequency multi-beam echo sounders (MBES) offer a solution to this problem by making faster measurements over larger areas. While these systems are primarily intended for high-resolution bathymetry, acoustic inversion techniques can be used to estimate seafloor parameters relevant to the UXO problem. The objective of this research is to develop and rigorously test a physics-based algorithm that can invert high-frequency acoustic data for sediment parameters. The result is a collection of new algorithms for high frequency acoustic data inversions and system-independent environmental assessment in terms of measurable seabed parameters, which can then be used as inputs to acoustic and electromagnetic systems.

Technical Approach

The inversion algorithms developed here incorporate the results of recent research in high-frequency sediment acoustics, utilizing both models and technologies that have been developed through ONR-funded experiments such as the Sediment Acoustics Experiments 1999 (SAX99) and 2004 (SAX04). To develop and test the algorithms, acoustic data was collected during three field experiments:

1. The Gulf of Mexico Experiment in 2011 (GulfEx11),
2. The Target and Reverberation Experiment in 2013 (TREX13),
3. The St. Andrew's Bay Experiment in 2014 (BayEx14).

These field efforts were sponsored by both SERDP and ONR under several different programs and this project utilized the infrastructure and logistics of those efforts to collect data. In each of these efforts, the acoustic data was collected using Seabat 7125 multibeam echo sounders that were provided along with technical support by Teledyne-RESON. The acoustic data collection in each of these experiments was accompanied by extensive environmental characterization in order to evaluate the accuracy of the inversion algorithms.

Results

While the data collected during GulfEx11 provided the basis for developing the inversion algorithm and to learn what was needed to collect a quality dataset, equipment problems, the abundance of fish, and saturation of the MBES data prevented the use of that dataset for inversion testing. The lessons learned during this experiment were applied to TREN13 and BayEx14 and helped to insure that the data was of sufficient quality to evaluate the inversion. The environments in both of these experiments were complicated, but the inversion performed well producing stable results that could be compared to ground truth measurements at the sites. These ground truth measurements were either compared directly to the inversion outputs or used in scattering models to compare to the inversion.

For TREN13, the inversion compared favorably to the ground truth measurements for a majority of the data products. Discrepancies between the scattering models and the inversion are most likely due to the inability of the scattering models to account for the multiple scattering from shell pieces at the site. The roughness spectrum obtained from the inversion compared well with the measurements across the entire test area for high wavenumbers indicating that the results would be applicable to modeling shallow grazing angle scattering for frequencies at least as low as 50 kHz.

The environment at the BayEx14 site was significantly more complicated than the TREN13 site. The presence of the mud layer and the transition layer between the mud and sand sediments was not accounted for in the inversion, which treated the seafloor as a half-space. Despite this approximation, the inversion results are stable and give effective parameters for the sediment that differ from the ground truth measurements. The scattering models, which incorporate the ground truth measurements, also do not account for the complexity of the environment and could potentially be modified to more accurately represent the scattering physics.

Benefits

Over the course of this project, the MBES inversion has reached a level of maturity that puts it at the cutting edge of remote seabed characterization particularly for the UXO detection problem. Taking a physics-based approach insures that the output of the inversion addresses the needs of modeling codes and simulations that incorporate similar physical models. This inversion algorithm and the data collection approach needed to apply it have the potential of being implemented into sonars without modifying existing hardware or software.

Objective

The objective of this research is to develop a technique that can be used with multibeam sonars to provide rapid, wide-area assessment of seafloor properties that can aid in the detection and classification of UXOs. While electromagnetic techniques have shown strong promise as a means of detecting and discriminating UXO from rocks and other debris, they must be close to the target in order to work well. This limits their capability in wide-area surveys of remediation sites and will need to be augmented by other technologies. Acoustic systems such as synthetic aperture sonar (SAS) may provide a complementary means of detecting UXO over a wide area, but the ability of this technique to discriminate and classify UXO is heavily influenced by the underwater environment in which they are operating. Sediment roughness and volume heterogeneity both contribute significantly to bottom reverberation, the dominant limiting factor for UXO detection and classification. Reverberation appears as a background in the total acoustic response, from which the target contribution is to be detected and classified. The ability of the sonar propagation and scattering models such as the PC SWAT to accurately model the reverberation depends on knowledge of the sediment properties.

Conventional techniques to measure sediment properties, such as stereo photography and sediment sampling, are time-consuming and labor-intensive. They also provide only point measurements, and multiple measurements are required to provide sufficient information about a complex environment. Remote sensing techniques using sonar have long been seen as a means of providing information about the seabed over large areas at potentially high resolution. The drawback to most implementations of sonar for seabed characterization is that they still rely on ground truth measurements to “calibrate” the algorithms used to identify seafloor types. In the end, these techniques don’t replace the point measurements, but instead supplement them by taking the information gleaned from the point measurements and mapping it over a wider area.

To truly be time and cost effective, the acoustic seabed characterization should work independently from any ground truth measurements. Evaluation of the sediment properties would then involve a single acoustic survey. For this approach to be viable, the acoustic inversion would need to be system independent and physics-based. Research into high-frequency acoustic interactions with the seafloor have progressed significantly over the last 30 years and has reached a level of maturity where this type of physics-based approach may be feasible. The objective of the research reported here is to develop such a physics-based algorithm and evaluate its performance using MBES data collected at three experiment sites. The ultimate goal is to develop the algorithm to a point where it can be integrated into the sonar processing suites, extending the capability of existing bathymetric sonars to include seafloor characterization. This type of system could address not only SERDP’s needs but also provide a valuable tool for marine habitat mapping and hydrographic surveys.

Background

Traditionally, the nature of the seafloor has been determined by means of direct sampling, photography, video, and various in-situ probing methods. Such measurements are time consuming and expensive when a large area is to be characterized. Acoustic methods have been developed with the aim of providing rapid coverage of large areas. Two commercially available methods have been widely used for over a decade. Though variants are available, these approaches are exemplified by QTCView™ [1]-[3] and Rox Ann™ [4]-[6]. These methods extract “features” from the sonar echo envelope and subject these to clustering analysis to classify portions of the survey area into several types. At this stage, the true nature of these types is unknown, as sonar echoes depend not only on the properties of the seafloor, but also on water depth and sonar properties. In order to identify clusters with specific seafloor types, acoustic surveys must be accompanied by ground truthing using methods such as grab sampling and video observation. If sufficient ground truth is available to include all seafloor types in the survey area, the clusters obtained from acoustic data can be identified with seafloor types. Where time and resources have permitted sufficient ground truthing, these methods have proven to be robust and useful.

As ground truthing requires extra resources and can be expensive and time consuming, there have been efforts to avoid this step by extracting echo features that are intrinsic to the seafloor and independent of such factors as water depth and sonar parameters. These methods employ physical models for acoustic scattering by the seafloor [7]-[10]. The power of this approach is increased when used with multibeam sonars, which typically provide more than 100 time series, one for each beam, greatly reducing inversion ambiguity.

The primary challenge in the approach presented here is that the models used must be sufficiently realistic and general to emulate a wide range of seafloor types. Our use of this approach in the SERDP application is supported by the successful development of a wide range of seafloor acoustic models by personnel of APL-UW [11].

Materials and Methods

In order to develop, test, and evaluate the sonar inversion algorithm, we collected both acoustic data for inversion and ground truth data to test the performance of the inversion. The systems used to make these measurements as well as the inversion algorithm itself are described below.

Teledyne-RESON Seabat 7125

The physics-based inversion algorithm developed during this project was not designed for use with a specific sonar system. It instead requires that the sonar be well characterized (calibrated source level, beam patterns, and well-understood pulse characteristics) and, for accurate results, have narrow beams and short pulse duration such that the interface and volume response of the sediment can be well separated. In order to collect data to test the inversion algorithm, for this project we chose to focus on the Teledyne-

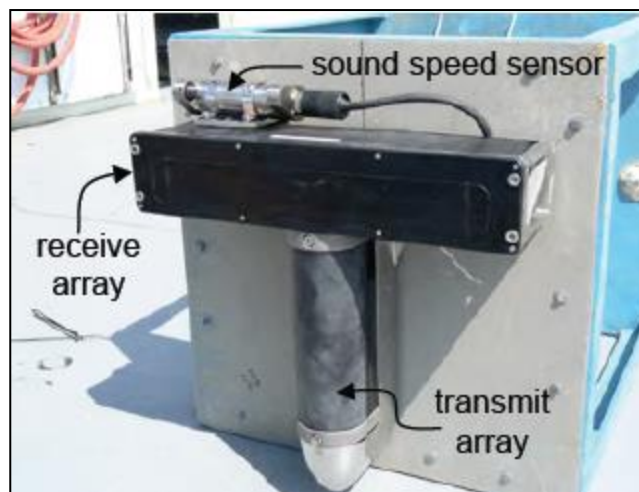


Figure 1: Teledyne-RESON Seabat 7125.

RESON Seabat 7125. This was a sonar system that has been used in other projects at APL-UW and by working with our colleague Dr. Gorm Wendelboe at Teledyne-RESON, we were able to use R&D versions of the 7125 for each of the field tests at no cost to the project. These systems had modifications and improvements that made them ideally suited for the data needed for this project and these improvements to the Seabat 7125 have since been incorporated into production models of the sonar.

The Seabat 7125 consists of a source and receive array as shown in Figure 1. The source projects a beam pattern on the seafloor that is very narrow along track and very broad across track. The receive array is oriented perpendicular to the source and the receive signal can be beam-formed to produce 256 beams each of which is broad along track and narrow across track. As a result, the signal measured for a given beam corresponds to the acoustic response of a small portion of the seafloor. Typically the time-of-arrival for that response is used to compute the distance to that patch of the seafloor and then used to produce high-resolution bathymetric maps. The full time series response of each ping can also be recorded as was done in each of the experiments discussed here and used in the inversion algorithms.

The Seabat 7125 is usually operated at either 200 kHz or 400 kHz depending on the depth of the seafloor. The beam width at 200 kHz is 2 degrees along track and 1 degree across track. The beam width at 400 kHz is 1 degree along track and 0.5 degrees across track. The beams extend across a full swath-width of 140 degrees. For this project, the software



Figure 2: The IMP2 (left image) and the SLS (right image).

used to run the 7125s was modified to operate at 20-25 kHz increments from 180 kHz to 420 kHz. The beam widths at each frequency varied between the two extremes at 200 and 400 kHz.

Environmental Characterization

While the inversion algorithm does not rely on ground truth data to identify the seafloor types, evaluation of the algorithm performance does require a separate measurement of the seafloor properties. This seafloor characterization was conducted during each field test to try using systems and techniques developed over 30 years of high-frequency acoustics research by APL-UW and our collaborators.

In-situ Measurement of Porosity 2 (IMP2)

The IMP2 is a sediment conductivity measurement system developed to support SAX99 and SAX04 [12], [13] (Figure 2). It uses a single constant-current electrode that is scanned through the sediment in a 2D plane using a horizontal and vertical positioning system mounted on a frame that rests on the seafloor. The probe can be inserted up to 25 cm into the sediment in 1 mm increments and at 1 cm horizontal steps up to 4 m. At each position the output voltage of the probe is recorded which is inversely proportional to the mean conductivity over the resolution cell of the electrode. The “formation factor,” F , is found by taking the ratio of the voltage measured in the sediment to the voltage measured in the overlying water. From the formation factor, the sediment porosity is calculated according to an empirical relation known as Archie’s Law,

$$\phi = \frac{1}{F^{1/m}}, \quad (1)$$

where m is a constant for a given sediment. This constant is determined by calibrating the probe using a sediment sample that is later dried and weighed to determine the bulk porosity. The spatial distribution of the porosity fluctuations can then be calculated and, if the sediment material properties are known, the density fluctuations can also be

calculated. These are used to determine the fluctuation power spectrum, which is used as an input to perturbation theory for volume scattering from the sediment.

Seafloor Laser Scanner (SLS)

The SLS is a structural-light-based system. It consists of a waterproof laser line projector, charge-coupled device (CCD) camera, and PC control unit [14] (Figure 2). The scanning head assembly maintains the relative position and orientation between the camera and the laser line source. The camera is a Basler A102f CCD with a resolution 1388×1038 pixels. The laser wavelength is 635 nm and a cylindrical lens is placed at its tip to generate a 60-degree fan angle.

The camera, projector, and housing are mounted on the IMP2. The SLS scanning head assembly is mounted on the horizontal linear stage, roughly 75 cm above the seafloor, to achieve an effective scanning swath width of 30 cm. The optical resolution on the scanning plane (across track) is 0.3 mm. In each image frame, the high-contrast pixels correspond to the reflection of the laser line from the seafloor. With a calibrated camera, the pixels on the laser line can be converted into the actual dimension of the bottom profile at the scan location [15]. As the IMP2 linear stage moves, the laser is scanned along the track. The resolution along the track is approximately 0.5 mm. This results in a digital elevation map (DEM) with an area of about $30 \text{ cm} \times 360 \text{ cm}$ with 0.3 and 0.5 mm resolutions across and along the track, respectively, and 0.1 mm in the vertical direction.

The DEM are used to calculate the 1D roughness power spectra from which the 3D power spectra can be determined by assuming that the roughness is isotropic. These 3D power spectra are then used as inputs for the small-slope interface scattering model for comparisons with the inverted interface scattering strengths.

Sediment Sampling

During each experiment, both diver cores and diver cofferdam samples were collected and analyzed. The diver cores are 5.9-cm-inner-diameter, polycarbonate plastic, cylindrical cores that are manually pushed into the sediment by a scuba diver. The top and bottom of the cores are capped and brought to the surface for later analysis. These analyses include measurement of the porosity, sediment density, and shell size distribution. Porosity was found by measuring the water-weight loss of the sediment by either drying the whole core or a section of the core at 105 degrees C for 24 hours. The sediment density was similarly analyzed by extracting the excess water from core, weighing, and accounting for the weight of the core and caps. The shell size distribution was assessed as a function of depth by sectioning cores and dry sieving the material in each section. The sieve sizes covered the range 1 mm to 9.5 mm. The material at a each sieve size was then weighed and counted to determine both the shell weight distribution and the number density.

Since the cores could only capture shell sizes less than 5.9 cm in size, larger cofferdams were also used. The cofferdams consisted of a plastic cylindrical pipe with a 21-cm-inner-diameter that could be inserted 10 cm into the sediment. The material within the

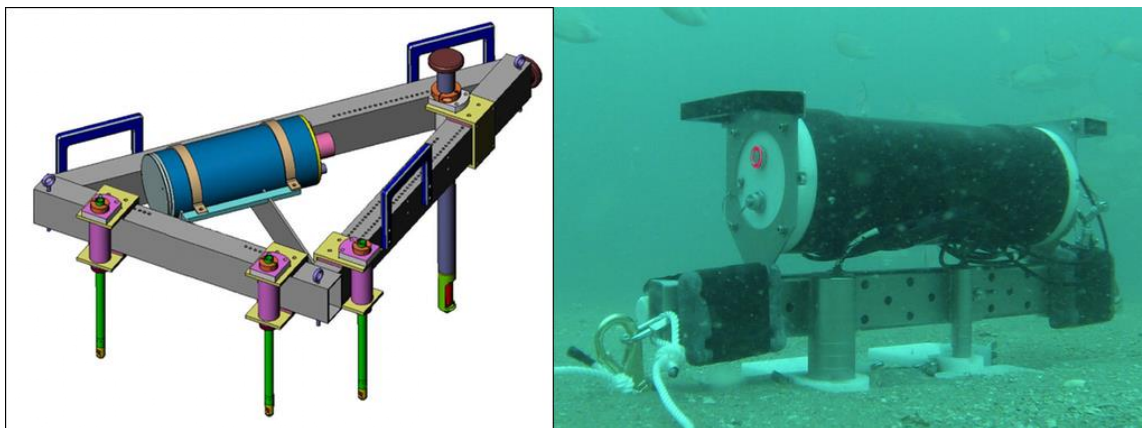


Figure 3: The "attenuation array" (left image) and the InSEA (right image).

pipe was then transferred to a mesh bag with 3 mm openings thus capturing only the larger shells and shell pieces. The collected shell was then dry-sieved and analyzed using the same procedure as was used for the diver cores shells.

"Attenuation Array" and InSEA

To measure sound speed and attenuation in the sediment, two different systems were used over the course of this effort. The first is called the "attenuation array" and was developed for SAX99 and SAX04 as part of the larger Sediment Transmission Measurement System (STMS1) [16]. The attenuation array consists of 2 sources and two receivers mounted at the ends of rods on a diver-deployable frame. The transducers feed into a junction box on the frame and are then cabled to the main STMS1 control unit. The diver pushes against the frame, driving the transducers into the sediment, and then alerts the operator on the ship that the frame is in place. The operator then triggers the data collection and, once complete, asks the diver to move the frame to a new location. During data collection, one source transmits from 40 – 100 kHz while the second source transmits from 100 – 300 kHz. The receivers are placed at different distances from each source and the sound speed is determined by the difference in arrival time at each receiver. The attenuation is determined by taking the ratio of the amplitudes measured at each receiver and comparing them to the ratio measured when the unit is in water [17].

The Investigation of Sediments by Acoustics (InSEA) system is an improvement on the design of the attenuation array and was developed by Méthodes Acoustiques de REconnaissance de l'Environnement in conjunction with Dr. Laurent Guillon at the French Naval Academy Research Institute. The system is similar in design to the attenuation array with two sources and two receivers, each mounted in stakes that can be driven into the sediment by a diver. The benefit of this system is that all of the electronics are in a pressure case on the frame and the diver can initiate data collection by pressing a button on the case. The system is very portable and operation does not require diver communications, as is the case with the attenuation array. Funding from ONR-Global supported the deployment of this system during TREX13.

Inversion of MBES data

The ultimate goal of any seabed classification technique is to determine the intrinsic physical properties of the sediment such as density, sound speed, and porosity. In the acoustic detection of UXO on the seafloor, the signal-to-noise is going to be strongly affected by the amount of scattering due to seafloor roughness and volume heterogeneity within the sediment and these become important sediment parameters in their own right. As opposed to the empirical approaches used in other classification techniques, in the inversion developed here the acoustic data collected with a MBES is used to first obtain estimates of the interface scattering strength, volume scattering, and attenuation. These parameters are estimated by fitting a model for the echo intensity time series, as in [7]-[10]. This approach separates the interface and volume scattering, which is possible due to the high directivity of the multibeam sonar. The estimates of the interface scattering strength can then be used to estimate the roughness parameters and the impedance of the sediment. Further estimates of the sediment parameters such as porosity and density can be obtained by using these parameters with published empirical relationships. A key point to this technique is that all of these parameters do not rely on any additional measurements of the sediment such as a grab samples or in-situ sound speed measurements. This process is summarized in the flow chart in Figure 4 and discussed in detail below.

Preprocessing

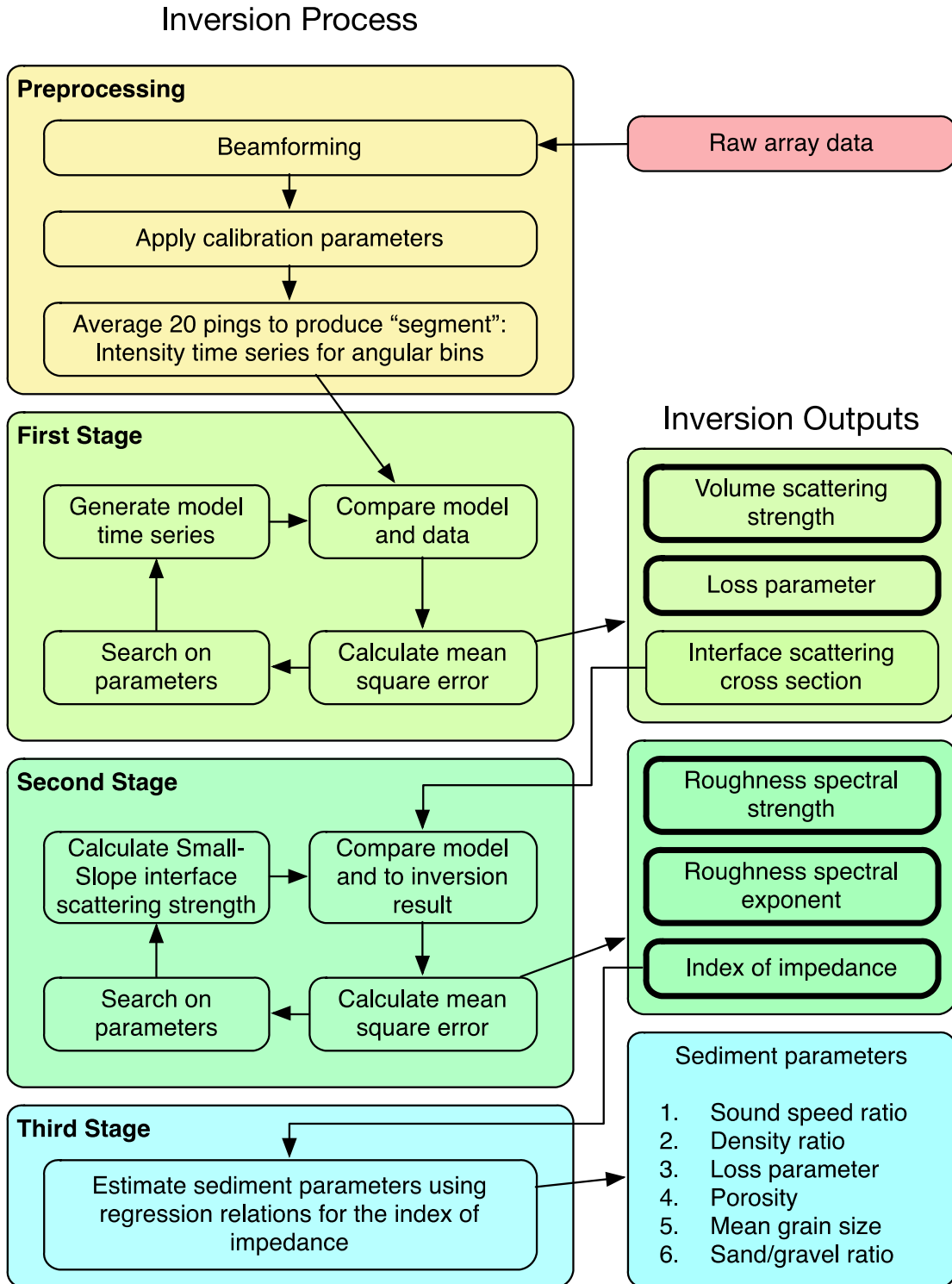


Figure 4: Inversion algorithm flow chart.

The multibeam echosounder is typically used to measure the seafloor bathymetry. In this application, the computer running the sonar beamforms the return for each ping and then extracts the profile of the seafloor from the envelope of that ping. The measured time series data are then either discarded or truncated about the seafloor return for future refinements to the bathymetry. In order to perform an inversion to extract the seafloor properties, the full time series data for each ping is recorded for later processing in MATLAB. A full implementation of the inversion processing capable of a wide area survey would perform this processing on the fly and, like bathymetric processing, would not require the user to retain the full, multi-element data.

The preprocessing of the data begins, as in the bathymetric processing, with beamforming (using Hamming weighting) with the beam directions fixed relative to the sonar and hence the ship. The time series for each beam is converted from complex to absolute values (envelope) and multiplied by calibration constants. These constants were measured by both Teledyne-RESON and APL-UW in their respective acoustic calibration facilities. With the calibration, the resulting time series is the mean-square relative pressure for a source giving unit RMS pressure at unit distance.

Once the calibrated intensity is found, the pings are collected into 20-ping sequential groups called “segments.” The 20 pings are further subdivided into four “batches” of five pings each. After aligning the leading edges of the envelope waveforms, an average is taken to determine the RMS envelope of each beam in each batch. Using these averaged pings, the effective roll of the ship is determined by looking across all angles and performing a linear fit to the bathymetric return as shown in Figure 5. The term

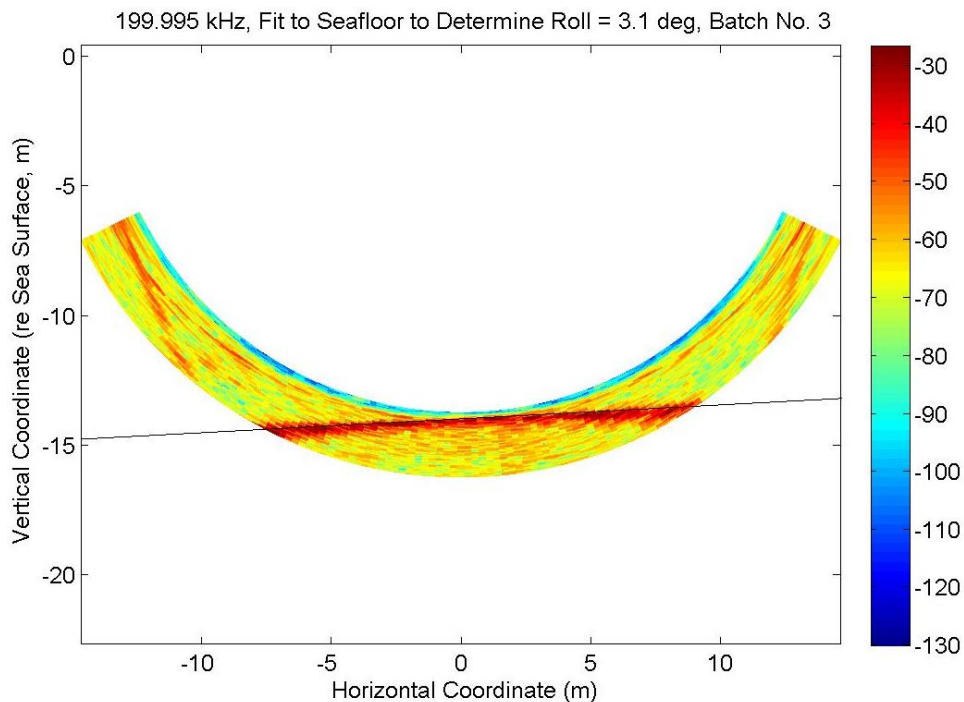


Figure 5: Linear fit to the bathymetric return in the beamformed MBES data. This linear fit determines the effective roll of the ship relative to the seafloor.

"effective roll" is used here since roll is usually defined relative to the true horizontal. In this application, the goal of the preprocessing is to determine the intensity data as a function of angle relative to the seafloor. The effective roll then determines the angular offset of the sonar relative to the cross-track seafloor slope. Once this offset has been applied to the data, the batches are reoriented to the seafloor normal and the data is placed in angular bins that are spaced by 0.5 degrees from 0 to 50 degrees off-nadir. Port and starboard angles are binned together and the bins only refer to the absolute value of angle from nadir. This increases the data for each scattering angle and simplifies the model-fitting procedure. At this point, the batches are averaged within each angular bin, and the data for each segment is reduced to 100 intensity time series as a function of angle.

First Stage

The intensity time series generated in the preprocessing are then fit in the first stage to determine the interface scattering strength, volume scattering strength, and attenuation. This fitting process is explained in detail in [18], but a brief summary is given here.

An inversion is performed for each segment. The first step in the inversion is to fit a simple time-domain sonar-equation model. The seafloor is assumed to be isotropic and is represented by a 2D distribution of point interface scatterers having angle-dependent interface scattering cross section and point volume scatterers with depth-independent volume scattering cross section. The attenuation within the sediment is assumed to be depth-independent as well. Time series are generated separately for each of the interface scatterers and for all of the volume scatterers. The responses from the interface and the volume are weighted by the initial guesses for the scattering strengths as well as losses due to effects such as spherical spreading and attenuation within the sediment. The source and receiver directivities are accounted for in the weighting function by integrating the product of the two beam patterns over the circle corresponding to the grazing angle of interest. Using theoretical beam patterns, which were found during calibration to be accurate at the beam angles of interest, a two-dimensional look-up table was generated assuming a fixed pitch for each field test that allows rapid generation of the time series. Figure 6 shows a typical time series generated using this approach where the volume echo is substantially separated in the time domain from the interface echo. This is due to the delay in the propagation into the seafloor and the effect of narrow directivity in limiting the time duration of the interface echo. This time separation is critical to the goal of quantifying interface and volume scattering as well as determining attenuation.

In fitting, a mean-square-error (MSE) cost function is used, and the fit is made simultaneously to a subset of the available angular bins (0 to 30° off-nadir). This fit is performed for each 20-ping segment. This fitting process gives the interface cross-section as a function of angle, volume scattering cross section, and attenuation for each segment. The MSE is quadratic in the two cross sections, so they can be found very rapidly by matrix inversion once a value is chosen for attenuation. The MSE is non-quadratic in attenuation, so to take advantage of the rapid inversion for cross sections, fits are performed for 10 values of loss parameter, δ , evenly spaced in the interval [0.001

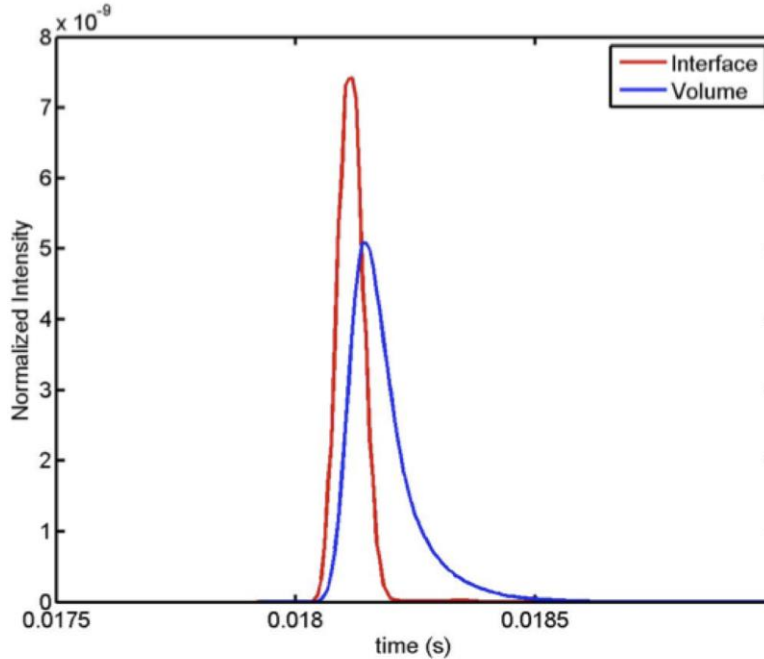


Figure 6: Example of model time series for interface (red) and volume (blue) scattering, 250 kHz, 8.5° off-nadir.

0.01]. The loss parameter giving the lowest MSE is chosen. The model does not include refraction, and cannot determine volume scattering cross section directly, as it is only sensitive to the product of the power transmission coefficient and volume scattering cross section. Thus nominal sediment parameters are used to give a rough value for the transmission coefficient. As the transmission coefficient only varies by approximately 0.5 dB over the expected range of sediment types (from mud to sand), the maximum error incurred is 0.5 dB when the nominal parameters are badly chosen. It is possible to refine this estimate after later stages in the inversion are completed. Interface scattering vs. angle is represented by a staircase function with step widths of 2.5° out to 30°. Data at shallower angles are not used, as the inversion becomes unstable. This may be due to a number of factors, such as neglect of refraction and ambiguity between interface and volume scattering at shallower angles.

At the end of the first stage, after fitting, values are obtained for each of the following parameters:

1. Interface scattering cross section vs. angle to 30° off-nadir
2. Volume scattering strength (depth independent)
3. Loss parameter (δ , depth independent)

Second Stage

In the first stage no physics is employed beyond that of the simple model, which is a sonar equation. In the next stage, the small-slope (SS) model (p. 334 in [11]) is fitted to the interface scattering strength found in the first stage. As SS requires sediment acoustic

parameters as well as roughness parameters, nominal values are used for density, sound-speed ratio, and loss parameter. The roughness spectrum is taken to be a pure power law with infinite outer scale,

$$W(k) = \frac{w_2}{k^{\gamma_2}}, \quad (2)$$

where k is the wavenumber, and a global search is performed for the spectral strength, w_2 , and the spectral exponent, γ_2 , to get the best fit to the angular shape of the scattering cross section while also determining the multiplicative factor needed to get a good fit. An example of this fit is shown in Figure 7. The multiplicative factor is used to correct the nominal impedance assumed at the outset. The corrected impedance is converted to Richardson's Index of Impedance, $IOI = \rho v_p$ where ρ is the sediment mass density in g/cm^3 and v_p is the sound-speed ratio.

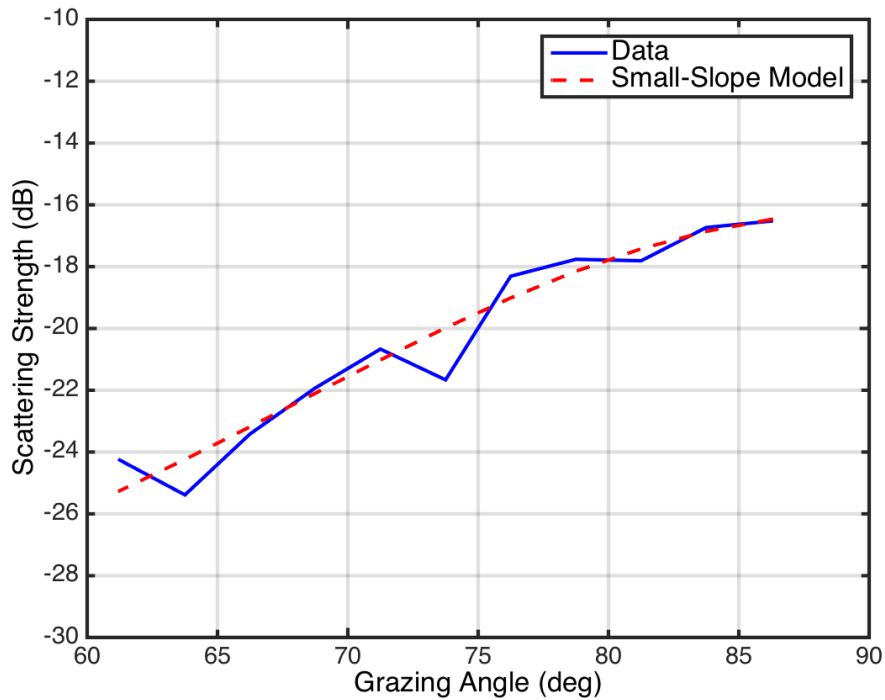


Figure 7: Example of fit of small-slope model to interface scattering strength obtained from inversion. This is the sand section of the TREX13 track; the frequency is 300 kHz.

At the end of the second stage, values are obtained for each of the following parameters:

1. Roughness spectral strength, w_2
2. Roughness spectral exponent, γ_2
3. Index of impedance, IOI

Third Stage

Using the *IOI*, the third stage utilizes empirical relationships between the physical properties of the sediment and the *IOI* derived from extensive measurements made on siliciclastic and carbonate sediments at 400 kHz. The relationships are expressed as regressions in Table 5.6 of [6] and are discussed extensively there. Since these regressions utilize the *IOI*, which is the product of the sound speed and density, the errors associated with these regressions are small ($r^2 = 0.96 - 0.99$). Since for these sediments, the sound speed is strongly correlated to the porosity, the errors associated with the porosity are also small ($r^2 = 0.99$). The loss parameter, mean grain size, and sand/gravel ratio have large errors associated with them and these are expected to have the greatest uncertainty associated with them in the final output.

The loss parameter obtained at this stage is redundant in that the loss parameter was already obtained in the first stage. The application to TREX13 and GulfEx14 indicates that the loss parameter from the first stage is smaller than the loss parameter from the third, perhaps because the latter includes scattering effects and the former is closer to the intrinsic value.

Using these *IOI* regressions, at the end of the third stage, values are obtained for each of the following parameters:

1. Sound-speed ratio, v_p
2. Density, ρ
3. Loss parameter, δ
4. Porosity, β
5. Mean grain size
6. Sand/Gravel ratio

Data vector

All of the outputs of the inversion process are summarized in the right hand side of Figure 4. In all there are 12 output parameters, only 5 of which are independent and thus suited for classification:

1. Volume scattering strength
2. Loss parameter from stage 1
3. Roughness spectral strength
4. Roughness spectral exponent
5. Index of impedance

These outputs are calculated for each segment and at each frequency.

Additional outputs

In developing the inversion and understanding its performance in different environments, several additional outputs have been examined and could potentially be integrated into a

final implementation. These outputs have to this point been used only qualitatively or to assess the performance of the inversion algorithm and hence have not been evaluated with the same rigor. They are presented here as possible future additions to this sediment classification scheme.

1. An additional output that is likely to prove useful is a 2D echo-sounder plot made using the nadir bin. This will be helpful in assessing layering and relative strength of scattering by interfaces.
2. Another output is conventional scattering cross section vs. angle, computed using the sonar equation under the assumption that all scattering is from the interface. Rather than using a simple $c\tau/2$ treatment of ensonified area, where c is the speed of sound in water and τ is the pulse width, the beam pattern azimuthal integrals employed in the more detailed model are used to avoid problems at near-nadir angles. This type of processing can be carried out to shallower angles than the inversions (to 50° off-nadir as of this writing). Penetration is so slight at the frequencies of interest that this scattering cross section agrees well with that obtained by combining the interface and volume contributions from the inversion.

Results and Discussion

In order to test and evaluate the inversion algorithm, three field tests were conducted: the Gulf Experiment in 2011 (GulfEx11), the Target and Reverberation Experiment in 2013 (TREX13), and the St. Andrew's Bay Experiment in 2014 (BayEx14). In each case, the work presented here took advantage of separate ONR and SERDP funded experiments to utilize the R/V Sharp for the deployment of the multibeam sonar and/or the systems used for the environmental characterization of the site. Also in each case, Dr. Gorm Wendelboe, a scientist with Teledyne-RESON, participated in the experiments providing both technical assistance and the multibeam sonar used to collect the data necessary to evaluate the inversion.

Gulf Experiment 2011 (GulfEx11)

In order to begin to develop and test the inversion algorithm, both acoustic and environmental data were collected in the Gulf of Mexico in the spring of 2011 prior to the start of this project. These measurements were collected while the R/V Sharp was in a four-point moor approximately two miles from Shell Island in Panama City Beach, FL during an ONR-sponsored pilot study for TREX13. The experiment site had a sandy seafloor and a water depth of 20 m.

While the R/V Sharp is outfitted with a MBES, Teledyne-RESON provided a calibrated Seabat 7125 multibeam sonar that was mounted in the well of the ship. The sonar was modified for operation at frequencies of 150, 200, 250, 300, 350, 400, and 450 kHz [19]. It employed a source having a narrow beamwidth in the along-track direction (1° at 400 kHz) and a cross-track beamwidth sufficient to cover the sector over which receiver beams were formed. The near-nadir receiver beams had a 0.5° cross-track width at 400 kHz. For frequencies of 250 kHz and lower, 128 beams were formed (from complex, element-level time series) to cover a cross-track sector of $\pm 64^\circ$. At 300 kHz and above, 256 beams were formed to cover this same sector. The sonar parameters were set to suppress time varying gain, the ping rate was 10 Hz, and pulse lengths were 160, 120, 96, 80, 69, 60 and 54 μs at the frequencies given above. Data were obtained in runs comprising 450 to 900 pings, with 10 to 15 such runs at each frequency. One objective was to obtain a large number of independent seafloor echoes for subsequent averaging and comparison with models. Although adjacent pings were quite similar in envelope shape, ship movement inside the moorings during each run was sufficient to provide the desired statistical population.

To test the inversion, several measurements were made of the environment at the experiment site. At the beginning of the experiment, the SLS was deployed from the R/V Sharp (Figure 8(a)) in order to measure the roughness of the seafloor. While the SLS is mounted on the IMP2, the conductivity probe was not working at the time of the 2011 experiment. The motorized trolley that positions the conductivity probe was working which allowed the SLS to collect a digital elevation map (DEM) over a 3.5 m long and 30 cm wide area on the seafloor with 1 mm horizontal resolution. A portion of the surface measured during the experiment in 2011 is shown in Figure 8(b) with the full DEM

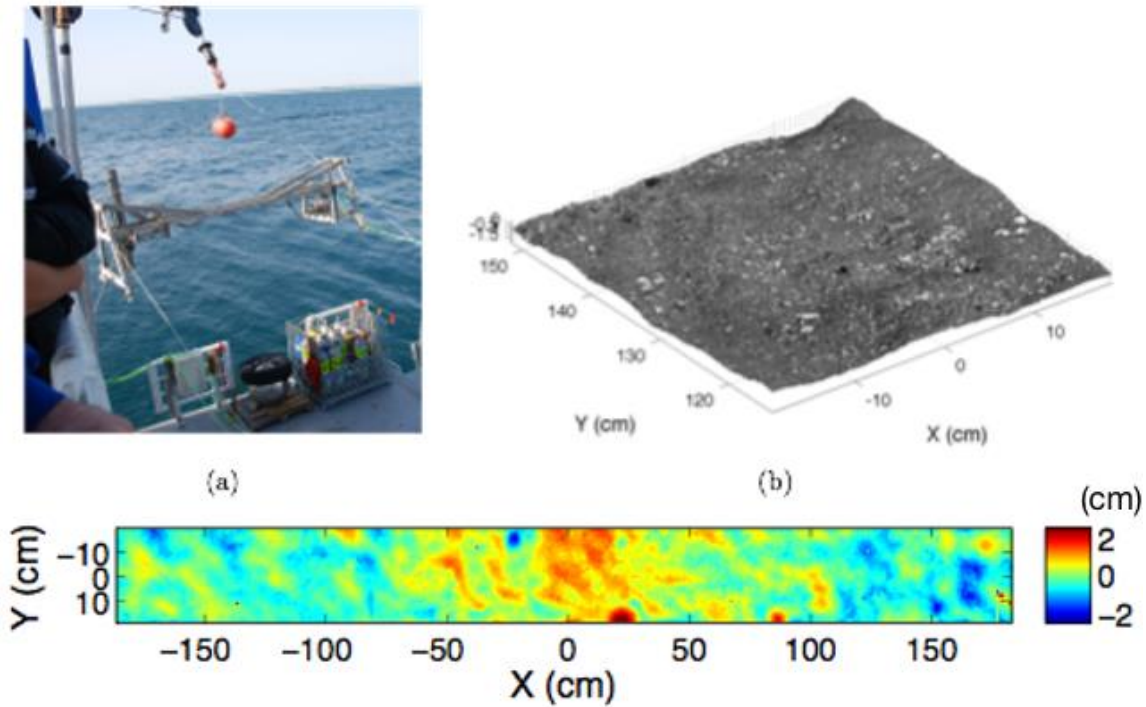


Figure 8: (a) IMP2/SLS being deployed during GulfEx11. (b) Example of a seafloor DEM measured during GulfEx11 with the laser line intensity superimposed to distinguish between shells and sand. (c) Complete DEM measured during a single SLS deployment at the experiment site.

shown in Figure 8(c). While the attenuation array was also deployed at this site, issues with the electronics prevented this data from being analyzed.

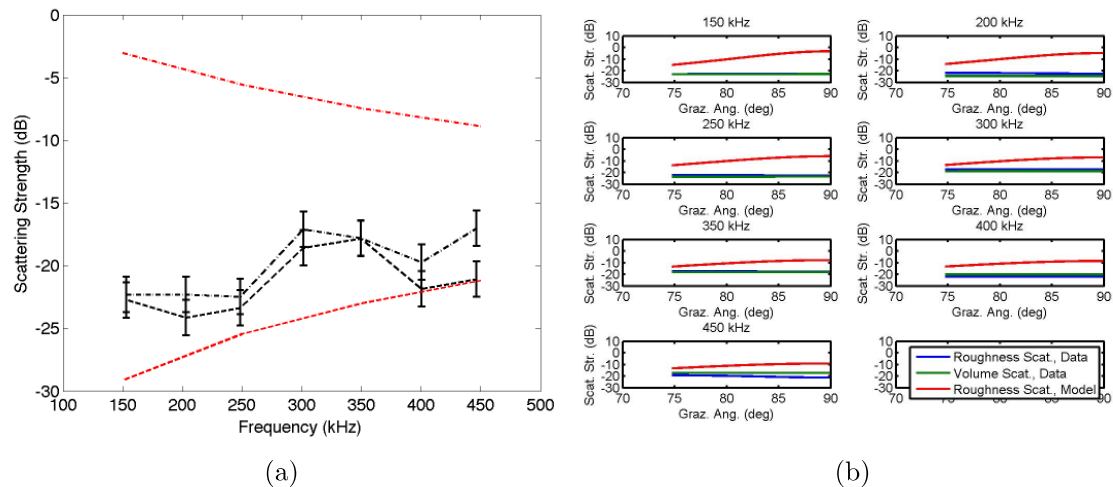


Figure 9: (a) Scattering strengths at normal incidence determined from the inversion (black lines) and the environmental characterization (red lines). For both the red and black lines, the interface scattering strengths are shown as the dot-dashed lines and the volume scattering contribution is shown as the dashed lines. (b) Scattering as a function of grazing angle for each frequency.

Although there was limited environmental data collected at the GulfEx11 site, the roughness and acoustic data were sufficient to begin to develop and evaluate the algorithm. In order to judge the repeatability of the inversion process and to gain a rough estimate of statistical error, data from three MBES runs at each frequency were used in three separate inversions. The resulting scattering cross sections were averaged and the average was converted to dB. Normal-incidence scattering strengths are shown in Figure 9(a). The error bars were computed by combining the standard deviation of scattering cross section from the three runs with a systematic error of 2 dB, obtained by a somewhat subjective estimation of errors arising at each stage in processing and fitting. There is a slight upward trend with frequency, though this trend does not appear to be statistically significant. The interface and volume contributions are similar, but scattering at the interface appears to be slightly stronger. As noted above, the volume contribution is comprised of contributions from two layers, but the final results gave no indication that layering is important, that is, the volume scattering strengths of the upper layer and the remainder are comparable.

We can estimate the scattering due to surface roughness at the experiment site [20]. Figure 10(a) shows the roughness power spectrum determined from the DEM shown in Figure 8. Using the power spectral fit, the Kirchhoff approximation can be used to obtain the red dot-dashed curve in Figure 9(a). The difference between the predicted surface scattering and the inversion results is on the order of 10 to 20 dB. This discrepancy was initially thought to be due to an issue with the roughness measurement. While the SLS has been extensively tested and undergone significant calibration, there is some uncertainty as to whether the surface measured by the SLS was the same surface seen by the multibeam. The SLS was deployed at the beginning of the experiment and, after several days, it accumulated a significant number of fish. This fish density reached the point where it not possible to collect roughness data due to the occlusion of the camera by the fish (Figure 11). As a result, the only useable roughness data was collected at the beginning of the experiment. The multibeam data was collected later in the experiment and by that time the fish that were attracted to the site most likely modified the roughness spectra. This was thought to account for the improvement in the scattering comparison for angles away from normal incidence, as shown in Figure 9(b), where the multibeam is scattering from areas of the seafloor where the fish did not rework the sediment.

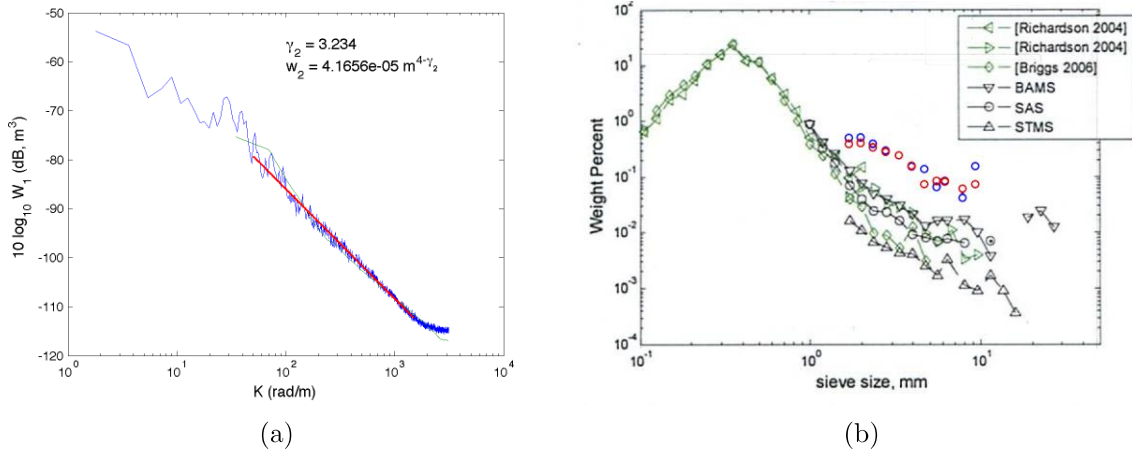


Figure 10: (a) Roughness power spectra determined from the DEM shown in Figure 8(c). The red line is a power law fit to the roughness spectra used to determine the two-dimensional power-law spectral fit, the parameters of which are shown. (b) The shell size distribution measured at the GulfEx11 site (red and blue circles) compared to the sand and shell distribution measured during SAX04.

Subsequent analysis of the multibeam data, however, indicates that the discrepancy may not be due to fish-induced roughness, but rather due to issues related to saturation of the multibeam data. Efforts to compensate for the saturated data may also be responsible for the areas of high scattering seen at angles far from nadir. These saturation issues are now well understood and were avoided during TREX13. While fish may not have been responsible for the scattering differences observed in this experiment, the presence of fish and their effect on the seafloor roughness remained an important consideration in planning for the 2013 experiment.

While the roughness scattering data/model comparisons may be affected by the saturation of the multibeam data, measurements of the shell size distribution at the experiment site, shown in Figure 10(b) indicate that shell pieces make up 3% of the sediment volume. This is significantly more than has been found in typical sand sediments which are on the order of 1% [21]. It is reasonable to assume that the majority of scattering from the sediment volume is due to scattering from the shell pieces. By treating the shell pieces as Rayleigh or geometric scatterers, the volume scattering strength can be estimated using the shell size distribution shown in Figure 10(b). The predicted scattering strength is shown as the dashed red curve in Figure 9(a). The comparison between the inverted and predicted values are much better for volume scattering than they are for roughness scattering with minor discrepancies at the lower frequencies. These



Figure 11: IMP2 and SLS late in GulfEx11.

discrepancies may be due to the presence of scattering from continuous volume heterogeneities that are not accounted for in the model. The discrete scattering inversion model also treats the shells in the volume and on the surface equally. The shells on the surface however may have both a different size distribution and a scattering response than those in the sediment.

As mentioned above, attenuation is obtained as part of the fitting process. The results shown in Figure 12 are consistent with typical values for sand. Apart from the dip at 200 kHz, the data are consistent with constant attenuation in dB/wavelength. This is equivalent to a linear rise in attenuation with frequency that is consistent with the frequency dependence measured in the laboratory and in other sand sediments. Due to problems with the attenuation array, attenuation was not measured at the experiment site and cannot be compared with the inversion results.

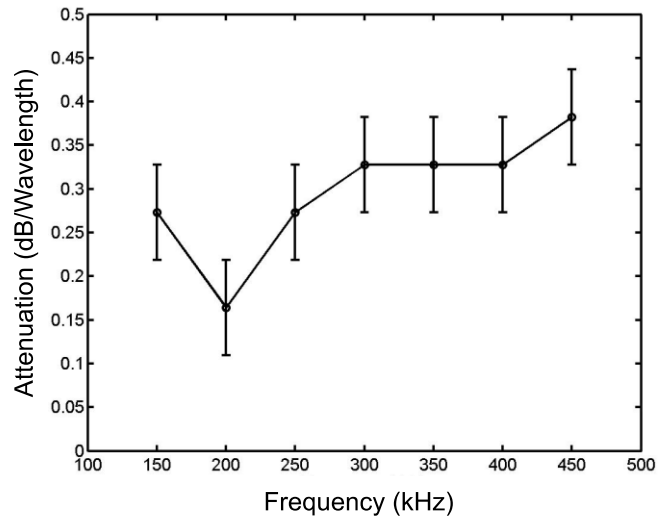


Figure 12: Attenuation at the GulfEx11 site found from an inversion of the multibeam data.

Target and Reverberation Experiment 2013 (TREX13)

The second field test took place in the spring of 2013 as part of TREX13. The main experiment was composed of two parts: an ONR sponsored reverberation experiment and a synthetic aperture sonar (SAS) target detection and classification experiment sponsored jointly by ONR and SERDP. The location and layout of the experiment is shown in Figure 13. A majority of the assets shown in the figure were deployed for the reverberation portion of the experiment while the SAS work took place at the moored location of the R/V Sharp at the intersection of the clutter and main tracks. The ship was in a four-point moor for a majority of the experiment, with the exception of the last two weeks when it was used to collect environmental and bathymetric data along the main track. It was during this time that we were able to utilize the ship to collect environmental and acoustic data along a 350 m line to the southeast of the mooring location. This line was chosen using the bathymetric and backscatter data collected by Dr. Christian de Moustier and Dr. Barbara Kraft during the survey cruise that took place immediately before the R/V Sharp was moored. As shown in Figure 14, the line starts at near the top of a ridge and traverses a swale as it moves towards the top of the next ridge. From the backscatter data, the ridge tops were areas of high backscatter while the ridge swales were areas of low backscatter. At the time it was believed that this indicated sand along the ridges and mud in swales and this location allowed us to collect data in both areas. This site was also far enough away from the mooring site so as not to be affected by the fish that had accumulated around the ship and the deployed instruments.

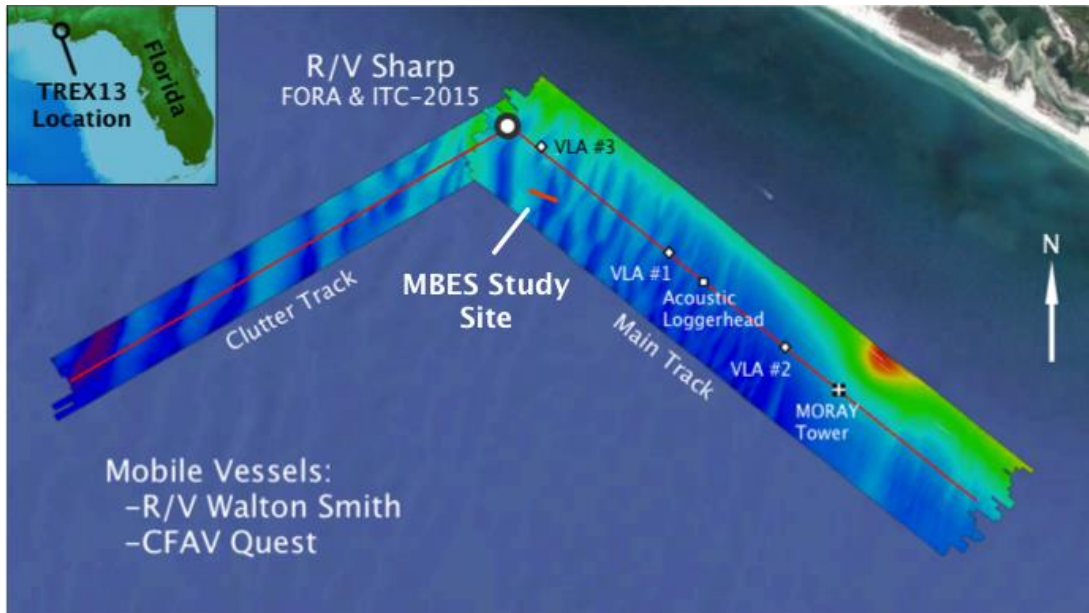


Figure 13: Bathymetry and distribution of assets for main reverberation component of TREN13. The location of the MBES Study Site to support the multibeam inversion work indicated to the southeast of the R/V Sharp.

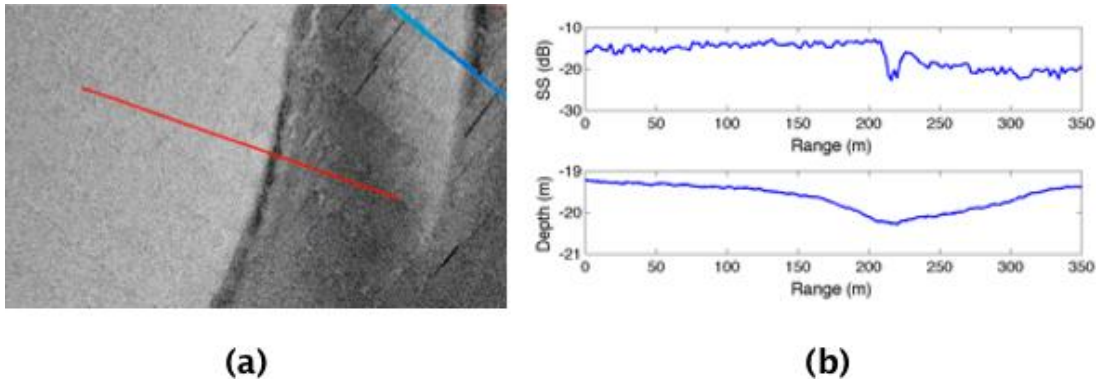


Figure 14: (a) Backscatter measured using the multibeam sonar during the survey cruise at the start of TREN13. The multibeam measurement track is shown as the red line. (b) The scattering strength (upper panel) and bathymetry (lower panel) along the inversion line.

The collection of MBES and environmental data took place from May 25 to June 4, 2013. The IMP2 and SLS was deployed along the track on May 25, multibeam data was collected along the track on May 27 and 28, and divers were deployed along the track on June 2 and June 4 to collect cores, samples, and deploy the InSEA. There were no weather events and no significant fish accumulation during this time.

MBES Data

For TREN13, Dr. Wendelboe brought two Seabat 7125s from Teledyne-RESON: the original system used during GulfEx11 and a newer prototype that had several

modifications that helped to avoid the saturation issues encountered during GulfEx11. Data was collected using both systems, but the latter system produced higher quality data that was eventually the focus of the inversion testing. Due to time limitations and to facilitate the deployments of both sonars, the 7125s were deployed using a pole mount on the side of the ship (Figure 15). While this enabled us to change out the sonars, this deployment configuration is unstable and can experience significant vibrations while the ship is underway. In an attempt to mitigate this issue, the ship used dynamic positioning to crab along the 350 m track at slow speeds (~1 kn). Also, since the sonar wasn't exactly aligned with the ship as would be the case in a well mount, there were unknown offsets in the pitch and roll of the sonar. The preprocessing for the inversion extracts the roll information so this isn't a problem, but the pitch does affect the inversion performance and was estimated through trial and error to be approximately 3°.

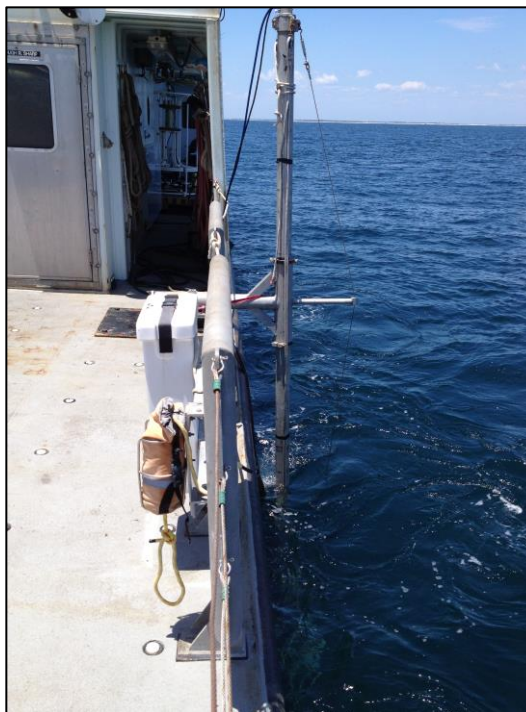


Figure 15: Pole mount used deploy the Seabat 7125 sonars from the R/V Sharp during TREX13.

Like the GulfEx11 sonar, the new sonar was also capable of operating at multiple frequencies and during this experiment both systems were operated at frequencies of 180, 200, 225, 250, 275, 300, 325, 350, 375, 400, and 420 kHz. For each frequency, the R/V Sharp started at one end of the track and crabbed slowly to the other end where the frequency was changed for the return trip. This technique is not amenable for a wide-area survey such as the bathymetric survey shown in Figure 13 but worked well over the small track to collect data to test the inversion algorithm.

Environmental Data

To evaluate the accuracy of the MBES inversion, environmental measurements were collected every 50 meters along the track for a total of eight locations as shown in Figure 16. Ideally every system and sampling technique would be used at each location, but due to logistical constraints and the limited time allotted for these measurements only a few sites were fully characterized. Table 1 lists each of the environmental measurements and at which locations they were made.

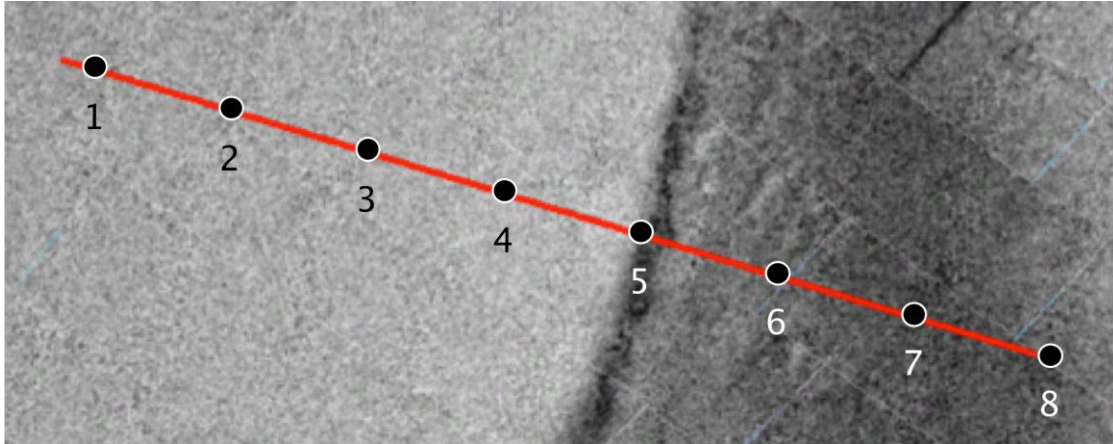


Figure 16: Locations of the environmental measurements along the MBES track.

System/Technique	Environmental Measurement	Sites
Conductivity Probe	Volume Heterogeneity	1,5,8
Seafloor Laser Scanner	Bottom Roughness	1,2,3,4,6,7,8
Diver Cores	Bulk Porosity Shell Size Distribution	1,4,5,8
Sediment Samples	Shell Size Distribution	1,4,5,8
In-Sediment Acoustic Probe	Sound Speed and Attenuation	1,4,5,8

Table 1: Environmental measurements and locations at along the MBES track.

Seafloor roughness was measured at all sites along the track except for site #5. In the backscatter data shown in Figure 17, site #5 lies on the edge of the line of extremely low backscatter. This region is mud that has collected at the base of the sand ridge and the IMP2's pads sunk 10-15 cm into this mud. This caused the laser line to be projected outside the field of view of the camera and data could not be collected. The 1D roughness power spectra measured at the other locations along the measurement track are shown in Figure 17. At the high wavenumbers, the spectra measured on the ridge are 5-10 dB higher than the spectra measured in the swale. Examination of the DEMs corresponding to these spectra indicates this higher roughness is driven by the shells which cover the seafloor on the ridge. These shells are absent in the swales and hence the interface is not as rough. Site #4 has significantly higher roughness due to the increase in the number of shells as the mud area is approached from the west.

In order to model the scattering from the seafloor due to roughness, the 1D roughness power spectrum at each site is fit by the sum of two spectra,

$$W_n(k) = W_a(k) + W_{bn}(k), \quad (3)$$

where n denotes the site number. For wavenumbers less than 30 m^{-1} , the spectra can be approximately described by the mean of all of the spectra along the track. Fitting a von Karman spectrum to this mean spectrum yields

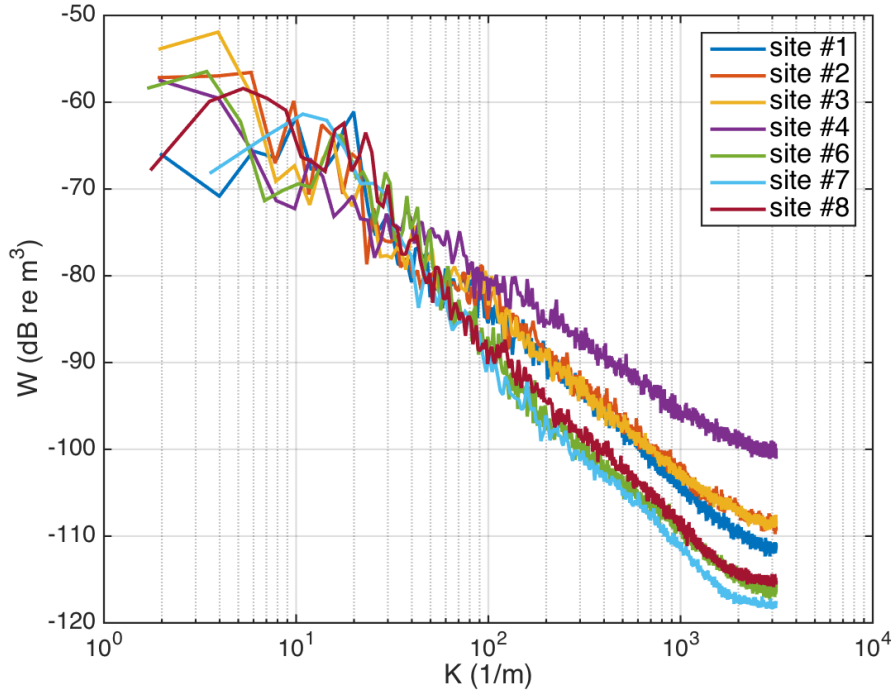


Figure 17: 1D roughness power spectra measured along the MBES measurement track.

$$W_a(k) = \frac{w_a}{(k^2 + L_a^{-2})^{\frac{\gamma_a}{2}}} \quad (4)$$

where $w_a = 0.003 \text{ m}^{(3-\gamma_a)}$, $\gamma_a = 4.23$, and $L_a = 0.1 \text{ m}$. For $k > 30 \text{ m}^{-1}$, the spectrum at each site is

$$W_{bn}(k) = \frac{w_{bn}}{(k^2 + L_b^{-2})^{\frac{\gamma_{bn}}{2}}} \quad (5)$$

where w_{bn} and γ_{bn} are determined from a power law fit at each site to the portion of the spectrum in the range $100 \text{ m}^{-1} < k < 1300 \text{ m}^{-1}$. The values from these fits are shown in Figure 18(a) and (b). The outer scale is chosen to be the same at each site, $L_b = 0.01 \text{ m}$. A comparison of this combined fit to the spectra measured at site #1 and #8 is shown in Figure 18(c). The 2D roughness power spectrum is required to calculate seafloor scattering using the small-slope approximation. Since the DEMs measured along the MBES measurement indicate that for the high wavenumbers the seafloor is isotropic, the spectral parameters for the 2D power spectra can be recovered from the 1D spectral parameters using Eq. (D.18) and (D.19) in [11].

The deployment of the SLS along the track took place over the course of a day and at several of the sites during its deployment, the conductivity probe was used to measure the porosity fluctuations in the sediment. While the variance of the fluctuations was found to be higher at site #1 than at site #2, in both cases scattering from these heterogeneities was

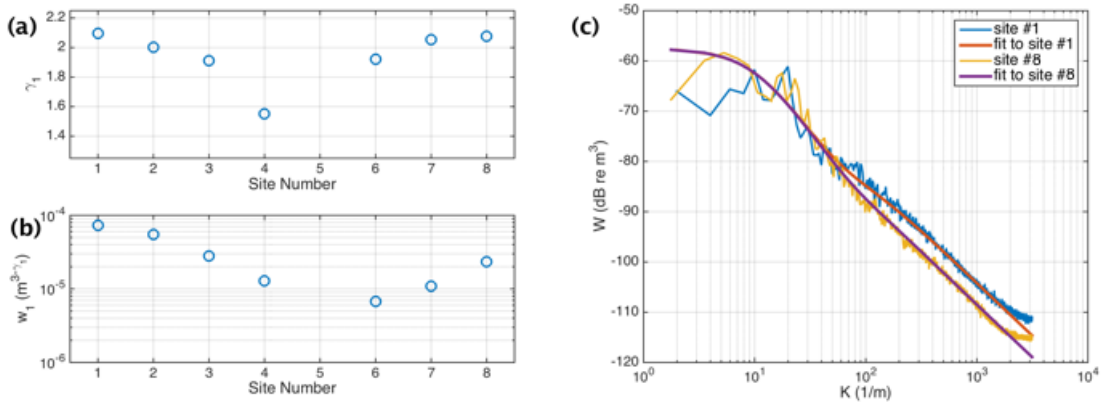


Figure 18: (a) Spectral exponent and (b) spectral strength determined from a power law fit to the roughness power spectra measured along the MBES measurement track. (c) Roughness power spectra and the spectral fits for sites #1 and #8.

Site	Density (g/cm^3)	Porosity	B ($10^{-5} 1/\text{m}^3$)	β
1	1.89	0.35	1.539	3.75
4	1.78	0.33	1.054	3.32
8	1.96	0.40	0.270	4.07

Table 2: Density and porosity determined from diver cores collected along the multibeam track.

predicted to be significantly lower than that due to scattering from the shell and shell hash within the sediment. As a consequence, this data has not been used in the inversion/model comparisons discussed below. At site #5, although the IMP2 footings sunk into the mud, it was still possible to deploy the conductivity probe and a 12 cm deep and 20 cm long set of data was collected in the mud. Inclusions of sand were observed in this data but there is too little data to collect meaningful statistics at this site.

Diver cores were collected at sites #1, #4, #5, and #8. Each of these cores was analyzed for sediment density, porosity, and shell distribution. The density and porosity determined from the cores are shown in Table 2. Site #5 is not shown since the mud area has not been included in the data/model comparisons. The shell weight distribution and the shell number density were determined from both the diver cores and larger cofferdams. The combined results of these measurements are shown in Figure 19. The density of the shell material was not measured, but a typical value of 2.7 g/cm^3 is assumed. Both the shell weights and numbers are consistent with the SLS measurements that indicate that the amount of shell increases as the mud area is approached from the west and then decreases abruptly at the mud area. The number density is the primary input to the scattering model used in the data/model comparisons. A power law has been fit to this data, as shown in the lower panel of Figure 19, which can be expressed as

$$\Psi_N = B a_0^{-4} \left(\frac{a}{a_0} \right)^{-\beta}, \quad (6)$$

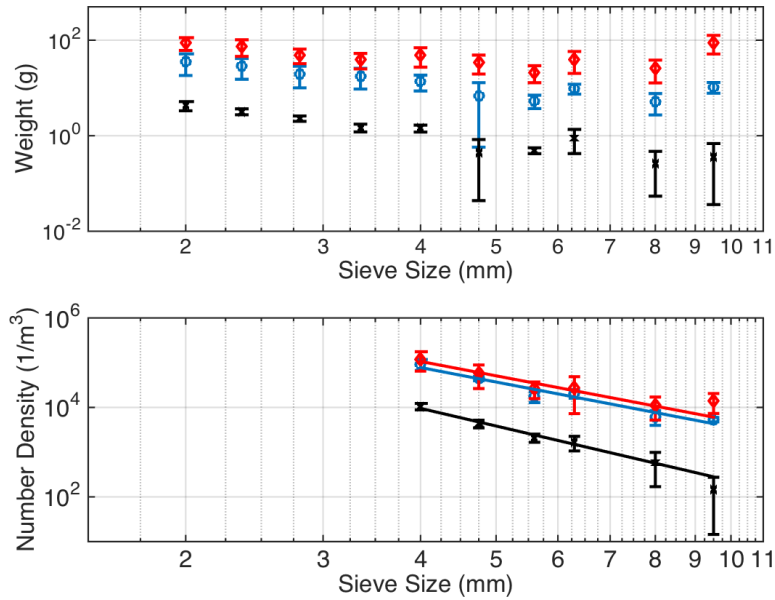


Figure 19: Shell weight distribution (Upper panel) and shell number density (lower panel) for site #1 (blue), site #4 (red), and site #8 (black).

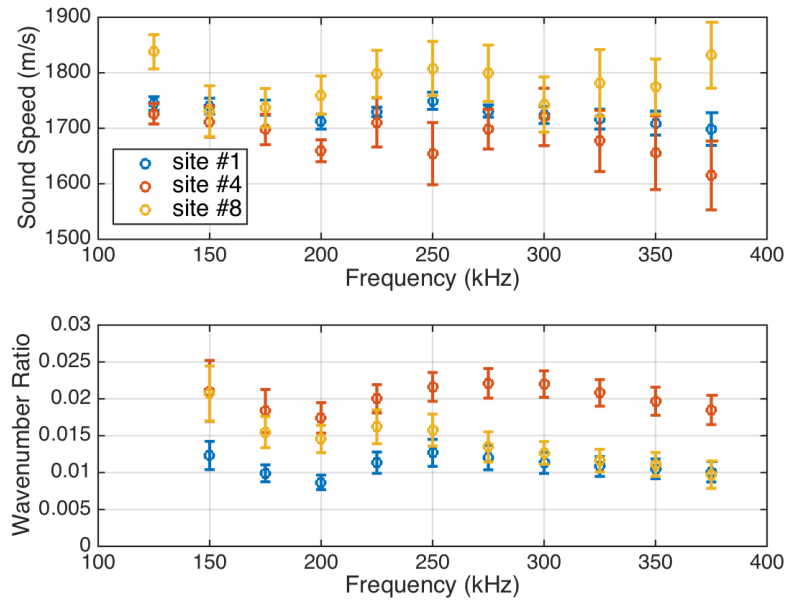


Figure 20: Sound speed (upper panel) and loss parameter or wavenumber ratio (lower panel) measured using the InSEA along the multibeam track.

where a is the shell radius in mm and $a_0 = 1$ mm. The values for the number density amplitude, B , and slope, β , are given in Table 2.

In addition to the diver cores, sediment sound speed and attenuation were also collected at sites #1, #4, and #8. The results of these measurements are shown in Figure 20, where

the sound speed and loss parameter (wavenumber ratio) are shown. The loss parameter is expressed as

$$\delta = \frac{k_p''}{k_p'}, \quad (7)$$

where k_p' is the real part of the sediment wavenumber and k_p'' is the imaginary part of the sediment wavenumber. The loss parameter measured using the InSEA captures both the intrinsic attenuation that would be present in a sand sediment in the absence of shells and the attenuation due to scattering from the shells in the sediment.

Inversion Results And Comparisons With Measured Predictions

To present the output of the inversion in a way that is consistent with the processing and useful to the user, the groups of segments are associated with patches of the seafloor along the data collection track. The inversion uses the beams from nadir out to 30 degrees on either side. These beams are used to produce the data vector discussed in the previous section and there is no direct angular dependence to the inverted parameters. The data associated with a given segment therefore corresponds to the portion of the seafloor of the seafloor interrogated by the 60-degree group of beams that for the TREX13 water depth corresponds to a 22 m swath width. In order to present the inversion in a meaningful way and to evaluate the uncertainties in the data, we have chosen to group the segments into square patches with the length of each side corresponding to the length of the swath width. Data from all of the segments within this patch are averaged and the confidence limits of the data are determined. An example of a map of the density values produced by the inversion along the TREX13 track is shown in Figure 21. This type of display (with multiple adjacent tracks) may be a final data product and visualization for the user in a future implementation of the inversion.

From the MBES inversion, there are five independent parameters which ideally could be compared to ground truth data in order to evaluate the performance of the inversion algorithm. Unfortunately, these outputs either do not correspond directly to a measurable quantity, as in the case of the *IOI*, or can be difficult to compare on a one-to-one basis, as is the case with the roughness spectral strength and exponent. For the roughness spectra, different values of the spectral strength and exponent can produce similar spectra over a limited range of wavenumbers. It is better in this case to compare the resulting spectra directly to determine how accurately the roughness spectrum has been determined and over what range the results are valid. We will therefore focus on 7 parameters for the inversion evaluation:

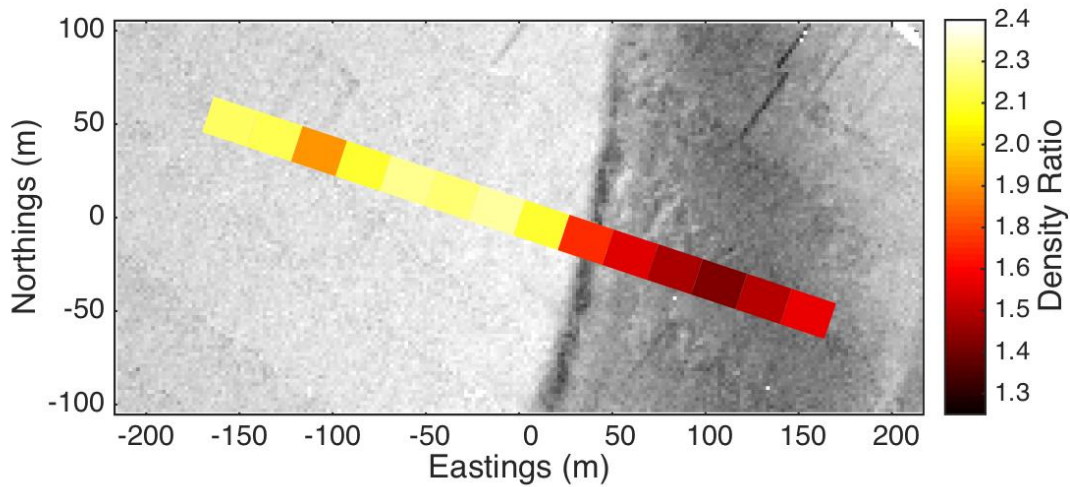


Figure 21: Map of the density ratio along the TREX13 track determined from the MBES inversion. The background is the scattering strength measured by de Moustier and Kraft during the experiment.

1. Volume Scattering Strength
2. Loss Parameter from Stage 1
3. Roughness Power Spectrum
4. Density Ratio
5. Sound Speed Ratio
6. Loss Parameter from *IOI*
7. Porosity

Comparisons of these parameters to the ground truth measurements are shown in Figure 22 – Figure 26.

A majority of the parameters are essentially frequency independent with the exception of the volume scattering strength, which is shown as a function of track position, and frequency in Figure 22. At each frequency there are a number of track positions where there is no data. To collect the MBES data, recall that the R/V Sharp crabbed back and forth along the track, collecting data at a single frequency for each run down the track. Moving slowly along the track made the ship susceptible to significant roll by the incoming swell and this, coupled with the instability of the mounting, corrupted some of the segments along the track. A rejection criterion was added to the inversion algorithm to remove these extreme events from the data. To invert for the frequency-independent parameters, the algorithm uses the data at all frequencies and as a result, the dropouts tend to be absent in these data products but they do increase the uncertainty in the estimate.

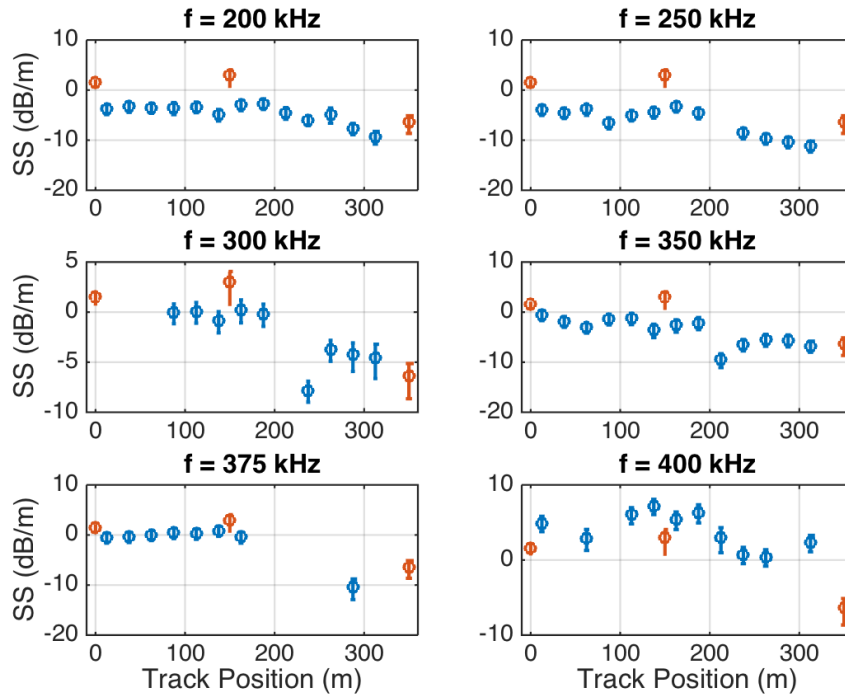


Figure 22: Volume scattering strength along the TREX13 track (blue) compared to model predictions made using the measured sediment properties and shell distributions (red).

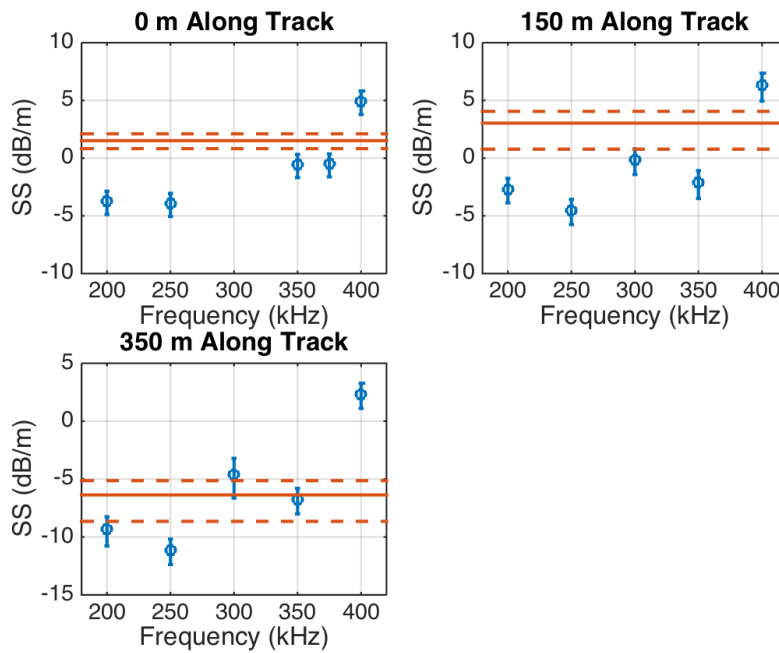


Figure 23: Volume scattering strength measured at 0 m, 150 m, and 350 m along the TREX13 track (blue) compared to ground truth predictions (red).

The volume scattering data is compared to predictions made using a discrete scattering theory developed by Dr. Anatoliy Ivakin [22], which uses as input the measured shell number density and sediment parameters (Figure 22 and Figure 23). The volume scattering model uses only the number density values measured along the track, which, as can be seen in Figure 19, extend from 3 mm to 9.5 mm. In reality, there are shells smaller than 3 mm but we've chosen not to extrapolate to these smaller sizes. The flat frequency response seen in Figure 23 is a consequence of this truncation of the number density at 3 mm. Extrapolating to lower sizes would produce a curve that increases with frequency and would be roughly 4 dB higher at 200 kHz and 9 dB higher at 400 kHz. These discrepancies between the volume scattering strength and the inversion for the portion of the track less than 200 m may be due to the failure of the volume scattering model to account for multiple scattering. There is significant shell content at this site and if multiple scattering were included in the model we would expect the scattering strength to decrease.

The inversion calculates the loss parameter at two different stages in the processing. The first takes place in the fitting procedure during the first stage while the second is derived from the *IOI* that is found in the second stage. Both of these results are shown as a function of distance along the track in Figure 24. The loss parameter from the *IOI* is roughly two to three times as large as that found in the first stage. The value from the *IOI* at the beginning and end of the track also compare well to the values measured using the InSEA. This is consistent with the hypothesis that the loss parameter in the first stage includes only the intrinsic attenuation and scattering from the shell pieces or other inhomogeneities is captured as volume scattering. For the InSEA, any energy scattered from the coherent field is lost in the measurement and manifests as additional attenuation. Since the *IOI* are derived from similar types of measurements, it is logical that the *IOI* loss parameter should also include scattering loss. This picture is not consistent however with the increase in attenuation at the end of the track where the shell content is significantly lower.

The roughness spectra produced using the spectral strength and exponent produced by the inversion are shown in Figure 25 as a function of range for $k = 100, 215, 464,$ and 1000 rad/m. Typically the roughness spectrum is shown as a function wavenumber as in Figure 18(c), but this type of plot makes it difficult to compare the inverted spectrum to the measured spectrum. Over this band of wavenumbers, the inverted spectra quite clearly capture the transition from shelly sand to the mud/sand side and the change in spectral level is comparable to the measured change. The absolute levels compare quite well at the highest wavenumbers while the inversion overestimates the spectra as the wavenumber decreases. At $k = 10$ rad/m (not shown in Figure 25), this overestimation is on the order of 10 dB. The cause of this divergence is not clear. In applying these results to a sonar system such as an SAS, which operates at shallow grazing angles, a bragg wavenumber of 100 rad/m corresponds to a sonar frequency of 12 kHz. At this frequency we would expect a roughly 5 dB error while for the lower two panels of Figure 25, we expect the inversion results to apply quite well to a sonar operating down to a least 50 kHz.

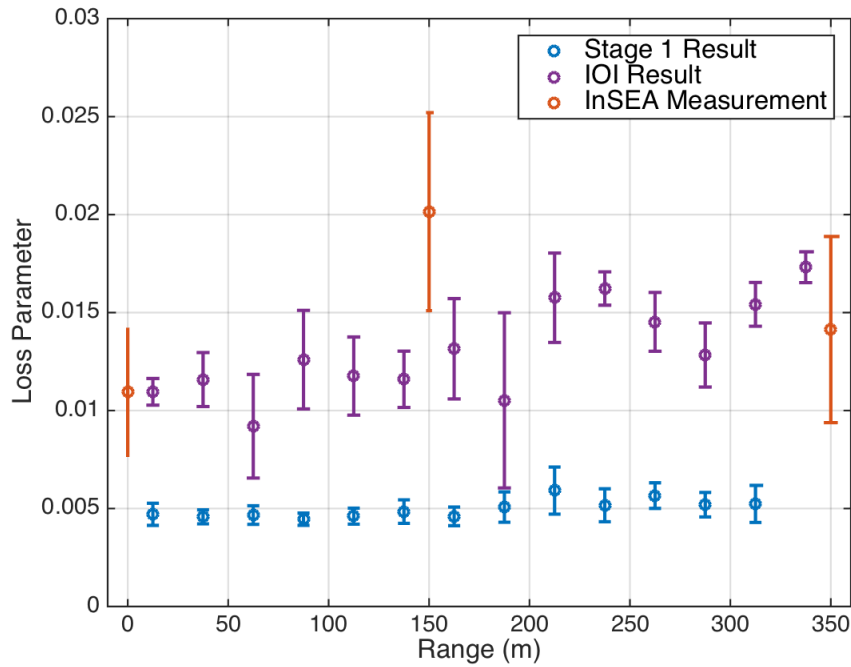


Figure 24: Loss Parameter determined from stage 1 of the inversion, from the inversion IOI result, and the InSEA.

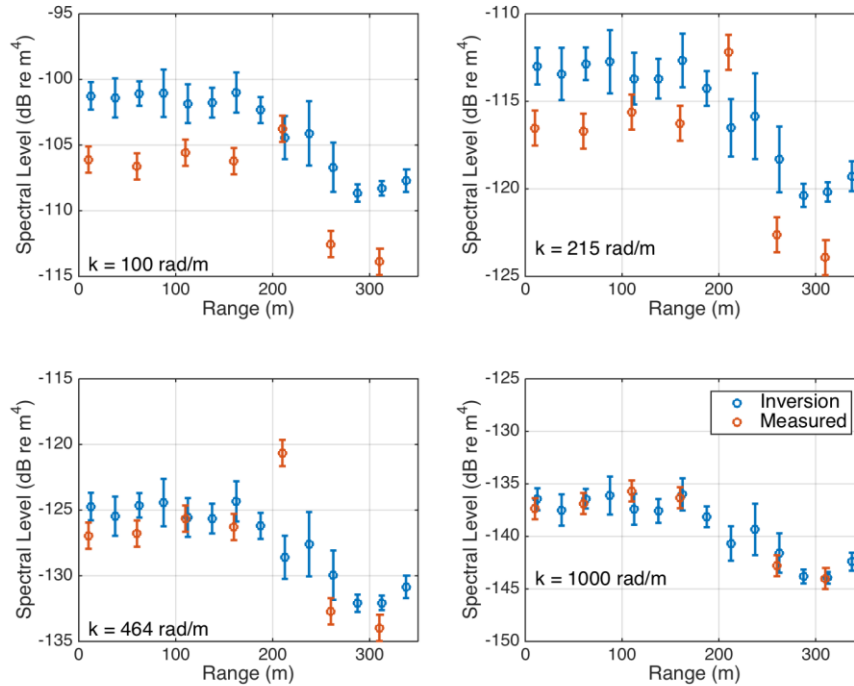


Figure 25: Roughness Spectra along the TRES13 track compared to the spectra measured using the SLS. Each panel corresponds to a different wavenumber.

Several of the values determined using the *IOI* from the inversion are shown in Figure 26. The *IOI* outputs compare reasonably well in the shelly sand area, slightly overestimating the values, but diverge significantly past the 200 m mark. The goal of this field test was to examine a sand sediment and, as a result, two of the three ground truth measurements were focused on the shelly sand side. The inversion appears to be tending towards the values measured at 350 m but there is not enough information in the 200 - 350 m range to test this aspect of the inversion here.

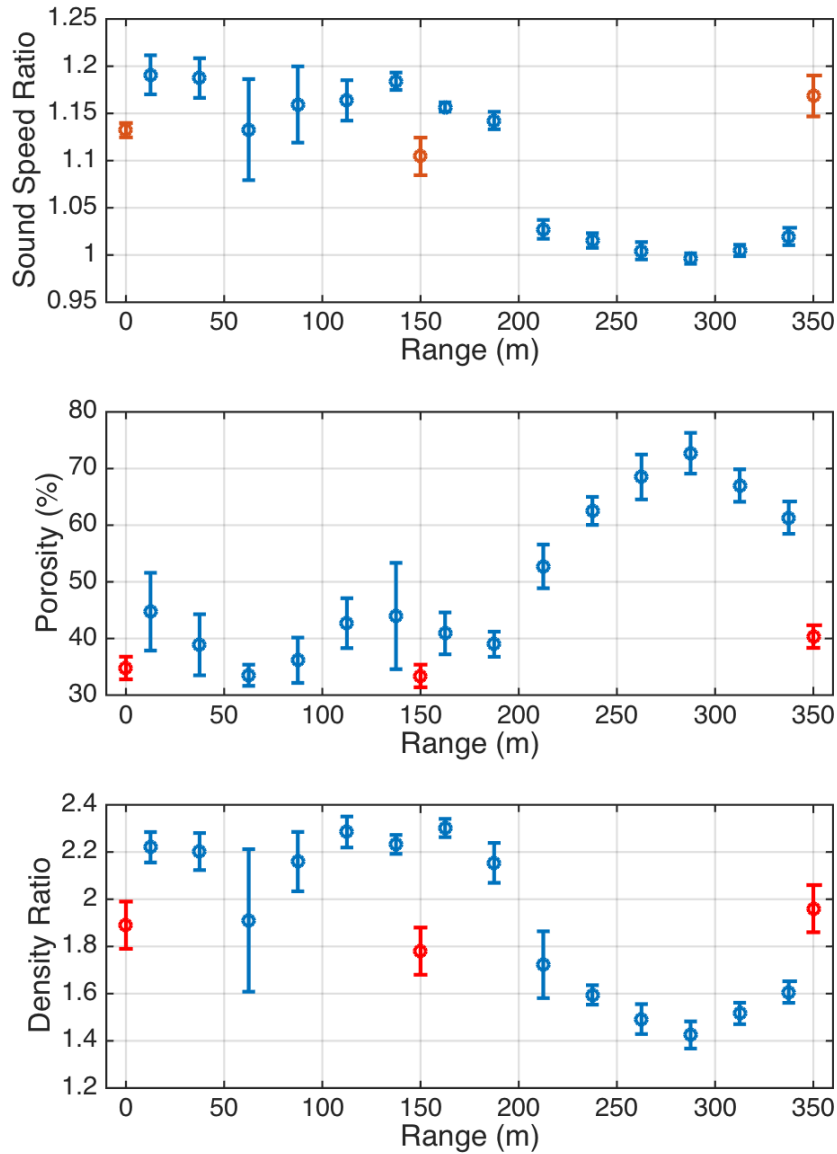


Figure 26: Sound Speed Ratio (upper), Porosity (middle), and Density Ratio (lower) determined using the inverted *IOI* (blue points). The measured values are also shown (red points).

Despite the instability of the MBES mounting during this field test, the inversion performed admirably in a trying environment. The TREX13 site is certainly a difficult one, much more so than a majority of sites visited in past high-frequency acoustic experiments. Multiple scattering seems to be prevalent, and the inversion model handles this problem gracefully. It fits a single-scattering model to multiple-scattering data. Codes such as PC SWAT also uses single-scattering approximations and, if it uses the inversion results as inputs, will produce the correct reverberation levels at our survey frequencies, if not substantially lower as indicated by the spectral inversions.

St. Andrew's Bay Experiment 2014 (BayEx14)

The third field test took place in the spring of 2014 as part of BayEx14. The main experiment was again focused on SAS target detection and classification and was jointly sponsored by ONR and SERDP. The location and layout of the experiment is shown in Figure 27. The R/V Sharp was again placed in a four-point moor for the entire experiment and the environmental measurements supporting the MBES inversion evaluation were conducted while the ship was moored. The location of the R/V Sharp was dictated by the needs of the main experiment and the multibeam data track was chosen to pass along the south side of the R/V Sharp location. The track was 200 m in length with the ship located at roughly the 100 m distance.



Figure 27: Configuration of the R/V Sharp and mooring lines relative to the MBES track. The inset shows the mooring location relative to the shoreline along the bay.

The collection of MBES data took place prior to the beginning of the experiment on March 30 and April 1, 2014 in order to collect data from the site prior to the deployment of equipment and the accumulation of fish. The ship entered the 4-point moor on May 8 and remained there until May 27.

MBES Data

For BayEx14, Dr. Wendelboe provided three Seabat 7125s: the original system used during GulfEx11, the system used during TREX13, and a new system that included design improvements over the TREX13 system. Data was collected along the MBES track with each system. The TREX13 sonar was a prototype in which Teledyne-RESON had been experimenting with new manufacturing techniques. As a result, the sonar performance had degraded between TREX13 and BayEx14 and we used the new system

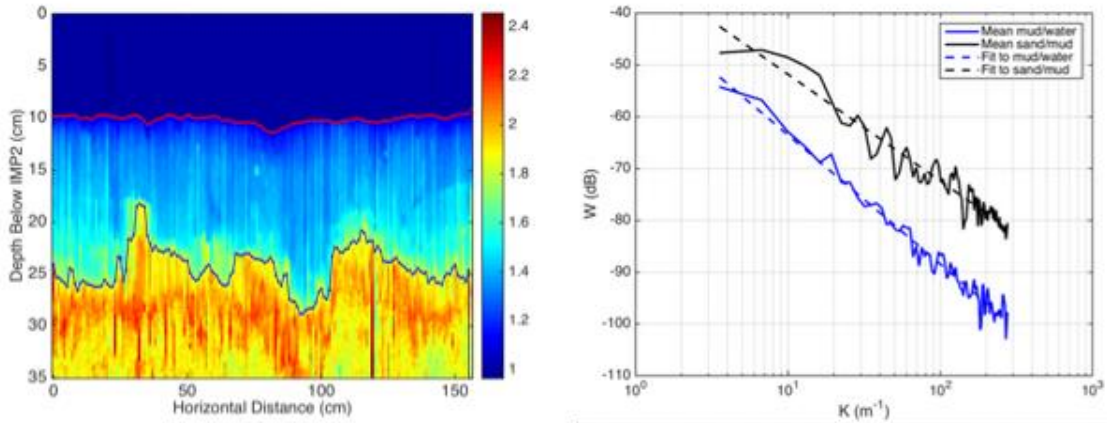


Figure 28: (Left panel) Formation factor measured using the IMP2 at the BayEx14 site. (Right panel) The mean spectra for the mud/water and sand/mud interfaces extracted from the formation factor data.

for the inversion evaluation discussed below. Instead of using the R/V Sharp to collect the MBES data, a dedicated survey boat was used to avoid the logistical issues that come with the use of the ship and to facilitate the deployment of the multiple sonars. The workboat was hired from Seaside Engineering and Surveying, LLC and was a 26-foot aluminum boat with a moon well for deploying the sonars. The bay was very calm during the data collection and, with the sonars mounted in the moon well, the data was of much higher quality than TREN13.

Environmental Data

The sediment in St. Andrew’s Bay at the BayEx14 site consisted of a mud layer over a sand/mud sediment. The mean thickness of the layer was determined from conductivity probe measurements to be 13.04 ± 1.25 cm thick. An example of a conductivity probe measurement at the site is shown in Figure 28. To measure the roughness of both layers, the formation factor data from the conductivity probe was processed to extract the 1D profiles of both interfaces. The mean spectra are shown in Figure 28 and the 1D roughness spectral strength and exponents are given in Table 3. The roughness spectrum for the mud/water interface agreed with the SLS measurements and the laser data showed that the power law continued to higher wavenumbers (<1000 rad/m). The sand/mud interface is very rough and is 5-10 dB rougher than the sediment at TREN13. This interface is also exceptional in that it is very difficult to determine exactly where the interface is located. The surface shown in Figure 28 is one an attempt to define the interface and alternative interpretation would be to define a mean surface and interpret the variations not as roughness but instead as volume heterogeneity. As will be discussed below, this may explain why the inversion overestimates the volume scattering expected for regions below the troughs of the mud-sand interface.

	1D Spectral Strength (w_l)	1D Spectral Exponent (γ)
Mud/Water Interface	$0.00014 \text{ m}^{3-\gamma}$	2.49
Sand/Mud Interface	$0.00075 \text{ m}^{3-\gamma}$	2.06

Table 3: Spectral strengths and exponents for the BayEx14 sediment interfaces.

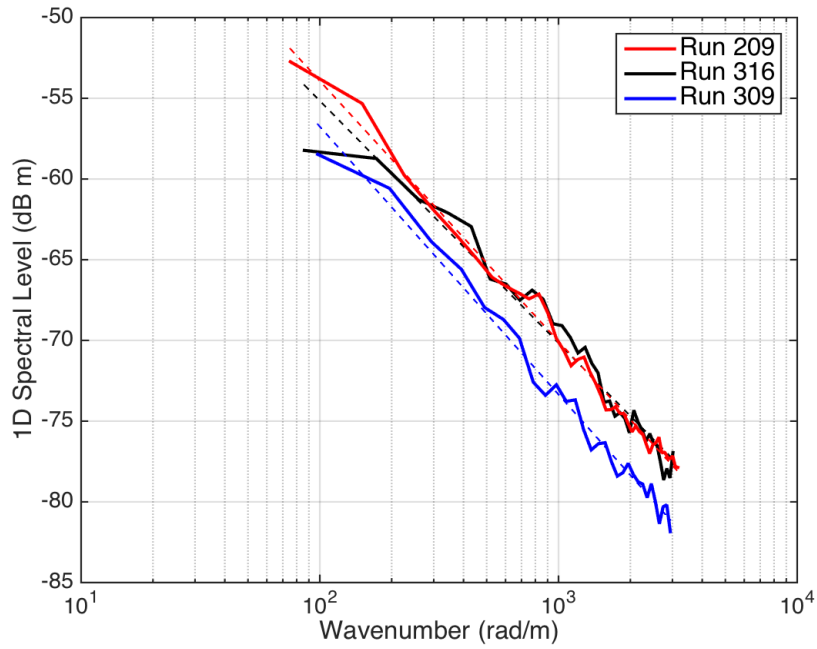


Figure 29: Density fluctuation power spectra within the underlying sand sediment.

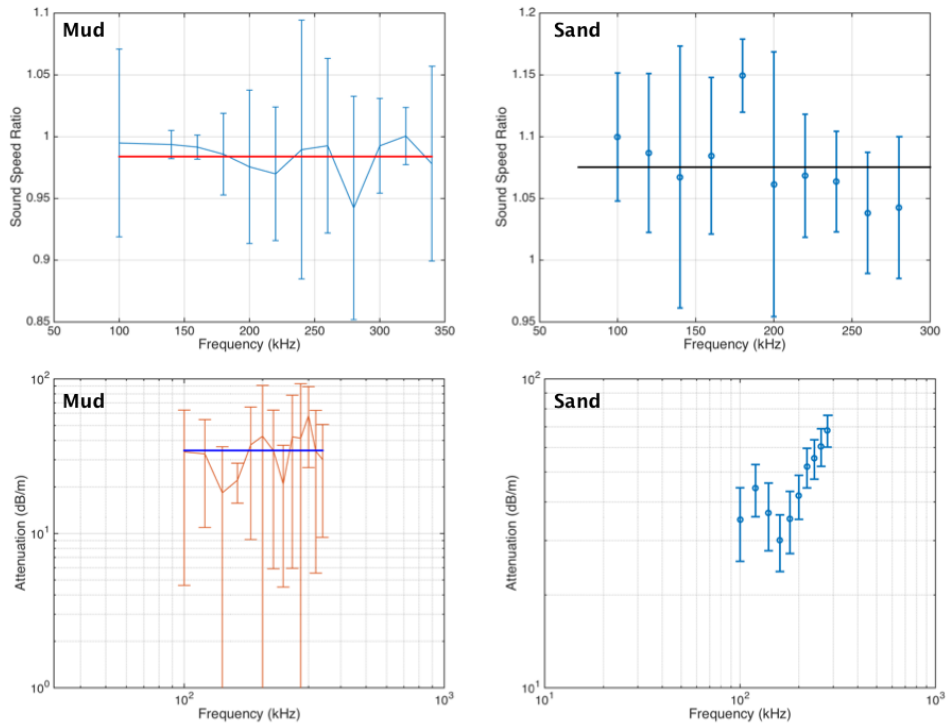


Figure 30: Sound speed ratio and Attenuation measured in the mud layer (left panels) and the underlying sand (right panel).

Diver cores were again used to measure the sediment properties, both in the mud layer and the underlying sand. There was no significant shell content in the underlying sand and the shell size distribution was not measured. The mud had a density of $\rho = 1.26 \pm 0.06 \text{ g/cm}^3$ and a porosity of $\beta = 81\% \pm 1\%$. The underlying sand had a density of $\rho = 2.10 \pm 0.02 \text{ g/cm}^3$ and a porosity of $\beta = 40\% \pm 1\%$.

Using the diver core data, the formation factor data from the conductivity probe could be inverted to get the density distribution in the mud layer and the underlying sand. The data was used to calculate the density fluctuation power spectrum shown in Figure 29. There were three different IMP2 data sets used to calculate the density fluctuation power spectra and the power law fits to each run yield the spectral parameters in Table 4. These measurements do not account for heterogeneities near the sand/mud interface which may be significant.

	Spectral Strength	Spectral Exponent
Run 299	0.0029 $\text{m}^{1-\gamma}$	1.75
Run 316	0.0031 $\text{m}^{1-\gamma}$	1.66
Run 309	0.0004 $\text{m}^{1-\gamma}$	1.50

Table 4: Spectral strengths and exponents for the density fluctuation power spectra within the sand sediment.

To measure the sound speed and attenuation in both the mud and sand layers, the attenuation array was deployed from the R/V Sharp. In order to measure the sound speed and attenuation in the mud layer, the array had to be reconfigured bring the receivers very close to the source. This greatly increased the uncertainty in the measurements as can be seen in Figure 30. In the mud, the mean sound speed ratio across the band was 0.984 ± 0.071 and the mean attenuation was $36.3 \pm 5.3 \text{ dB/m}$. For the sand measurements, one of the receivers was corrupted by cross talk and the processing had to be done using a single receiver. This introduced significant uncertainty to the sound speed ratio as can be seen in Figure 30 where the mean sound speed ratio is 1.075 ± 0.042 and a potentially large systematic bias to attenuation measurement, which has a mean of $46.1 \pm 3.8 \text{ dB/m}$. This value is potentially an order of magnitude too low.

Inversion Results and Comparisons With Measured Parameters

For the BayEx14 inversion, we will again focus on same the 7 parameters examined for the TRES13 inversion. Comparisons of these parameters to the ground truth measurements collected at the R/V Sharp position are shown in Figure 31– Figure 36.

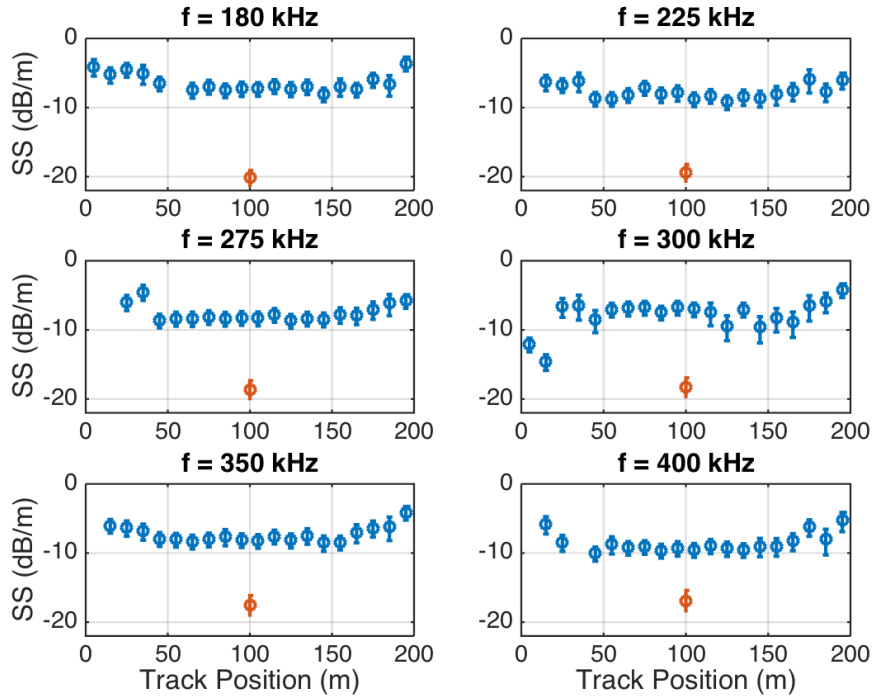


Figure 31: The inversion volume scattering strength along the BayEx14 track (blue) compared to scattering strength determined from the measured density fluctuations (red) in the sand sediment.

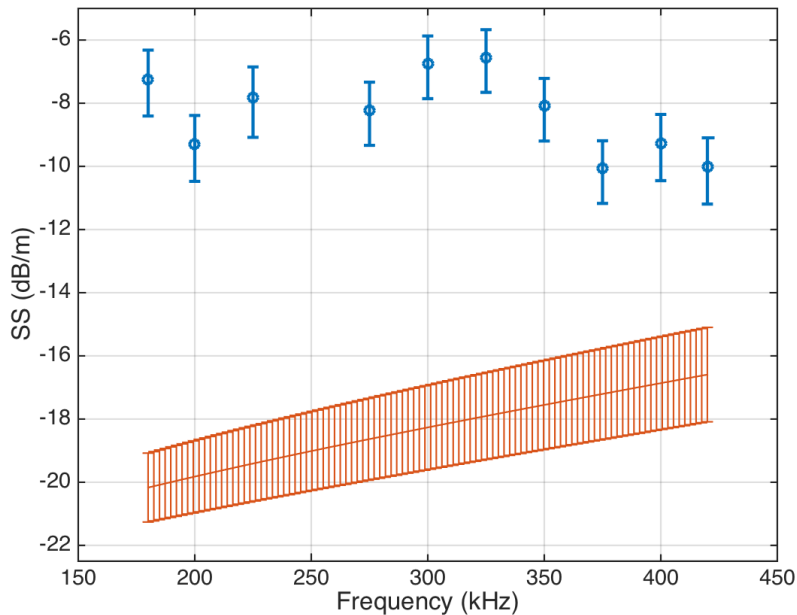


Figure 32: Inverted volume scattering strength (blue) at the 100 m distance along the BayEx14 track compared to the scattering predictions (red).

As opposed to the TREX13 inversions, the inversions for BayEx14 are much more stable; there are very few dropouts in the volume scattering strength along the track (Figure 31). The scattering strengths are also quite stable with only small variations (2-5 dB) along the track. The inversion seems to indicate that the ends of the track have a slightly higher volume scattering and roughness scattering response as can be seen in both Figure 31 and Figure 35. The volume scattering at the R/V Sharp site was calculated using small-perturbation theory (pp. 383-385 of [11]) using the sediment parameters and the fluctuation spectra in Figure 29. This assumes that the volume scattering comes entirely from the underlying sand sediment. The reasoning behind this modeling comparison follows from how the inversion is handling the mud layer. The inversion in its current state of development treats the seafloor as a half-space and is not currently equipped to deal with a layered medium. As a result, the processing interprets the first acoustic return as coming from the sand/mud interface, not the mud/water interface, and, in the first stage of the processing, the volume scattering is associated with this sand layer.

In this case, the scattering strength determined from the density fluctuations is under predicting the volume scattering by roughly 10 dB across the entire band and it is

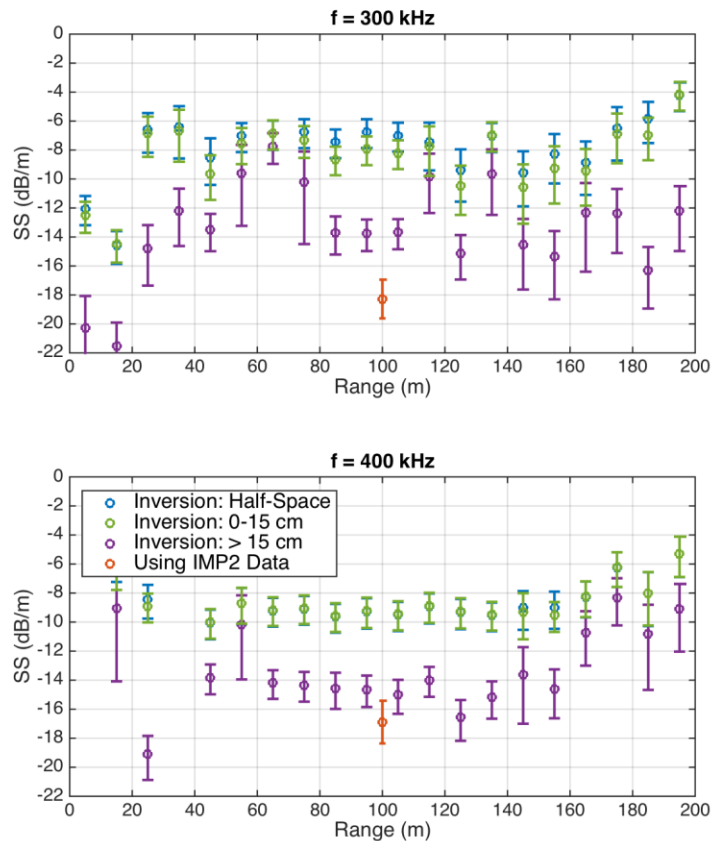


Figure 33: Results of a modified inversion which treats the top 15 cm of the half-space as a layer with different point volume scatterers from those scatterers below the layer.

difficult to say whether the inversion is failing or if the scattering model used to represent ground truth is incomplete. As opposed to a sand/water interface where the boundary is clearly defined, the mud to sand transition is much smoother as can be seen in Figure 28, and neither the scattering prediction nor the inversion currently accounts for this. This interface is also very rough, 5-10 dB rougher than TRES13, and it becomes difficult to discriminate between interface scattering and volume scattering along this interface since the boundary is no longer clear. The inversion may be treating this interface as volume scattering where the scattering based on the density fluctuations is not taking this into account. This hypothesis is also consistent with the spectral inversions shown in Figure 35 where the inversion slightly under estimates the sand/mud interface roughness spectrum.

This hypothesis is strongly supported by inversions that we performed using a more complex model. This model estimates volume scattering strengths for two regions, a 15-cm layer starting at the mud-sand interface and the half space below. This half space contains the regions in which the heterogeneity measurements leading to the red "ground truth" values in Figure 31 and Figure 32 were made. For the more complicated inversions, volume scattering strengths for the 15-cm layer are similar to those obtained from the simpler inversion, but those for the lower half-space agree with ground-truth within measurement uncertainties (Figure 33). Thus, the inversion agrees with ground truth when it isolates the region in which the ground-truth measurements were made.

At this stage it is clear that the more complicated inversion provides more realistic results, but it is not clear that the resulting complication is an advance in practical terms. First, the more complicated inversion used a "man in the loop", setting the 15-cm layer thickness. In a practical implementation, this setting could likely be automated, using the echo-sounder mode described earlier. Second, as noted earlier, the simpler inversion is consistent with the physics used in typical applications, such as PC SWAT, and will give the correct reverberation levels, even if some of the inverted parameters are somewhat non-physical. Our experience indicates that this situation will only arise in difficult environments like that of BayEx14, and not in the majority of cases.

The results from the *IOI* shown in Figure 34 and Figure 36 indicate that the sediment is mud; The density ratio, porosity, and sound speed ratio all compare very well with the values measured in the mud layer. The loss parameter in Figure 34 does not show the

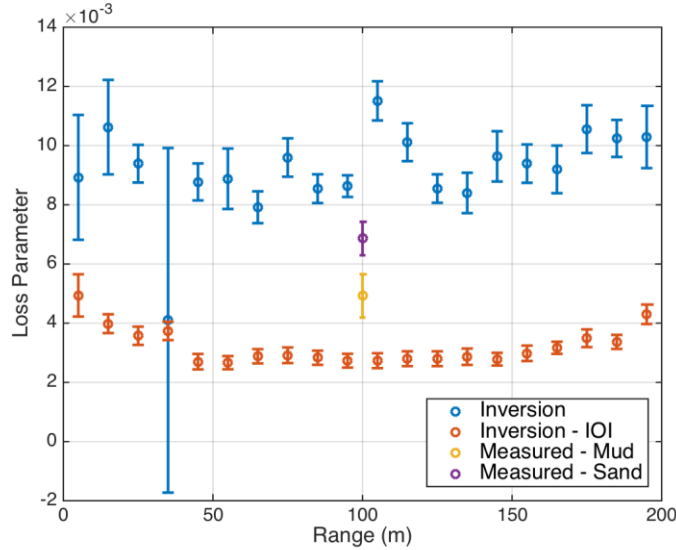


Figure 34: Loss Parameter determined from stage 1 of the inversion, from the inversion *IOI* result, and the attenuation array.

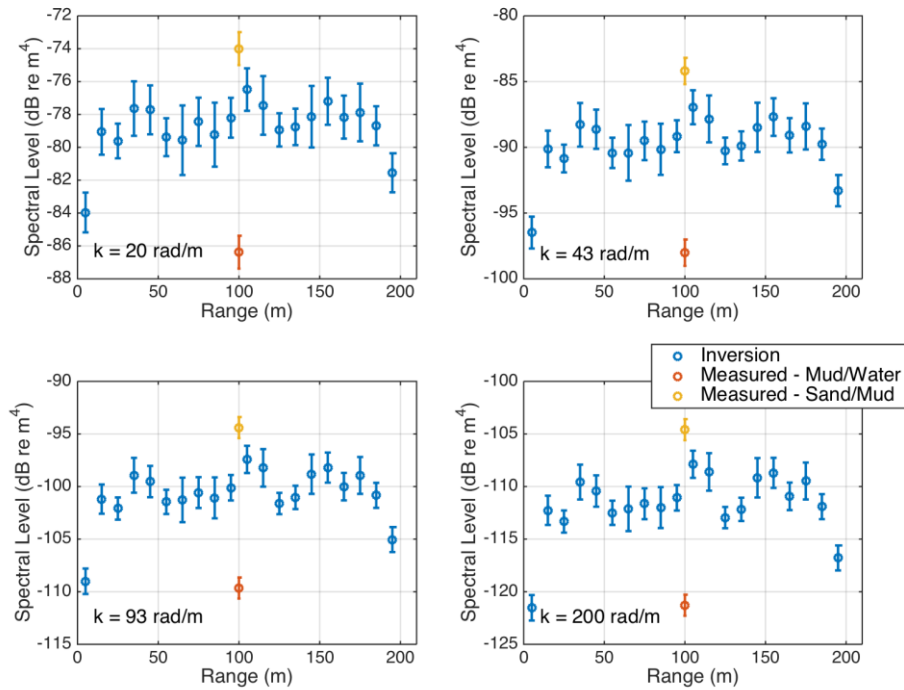


Figure 35: Roughness Spectra along the BayEx14 track compared to the spectra measured using the SLS. Each panel corresponds to a different wavenumber.

same agreement but the attenuation measurements in both the sand and mud are unreliable and the values given from the *IOI* regressions are consistent values for other mud sites. Again this seems surprising given that the inversion is seeing the sand/mud layer as the start of the half space, but the conductivity probe measurements indicate that this boundary is not abrupt but that there may be a transition layer where the sand-to-mud ratio gradually increases across the boundary. This kind of transition layer has been shown to greatly reduce the reflection coefficient [23], particularly near normal incidence, which could lead to a reduction in the *IOI*.

It appears that both the inversion and the scattering models fail to account for the

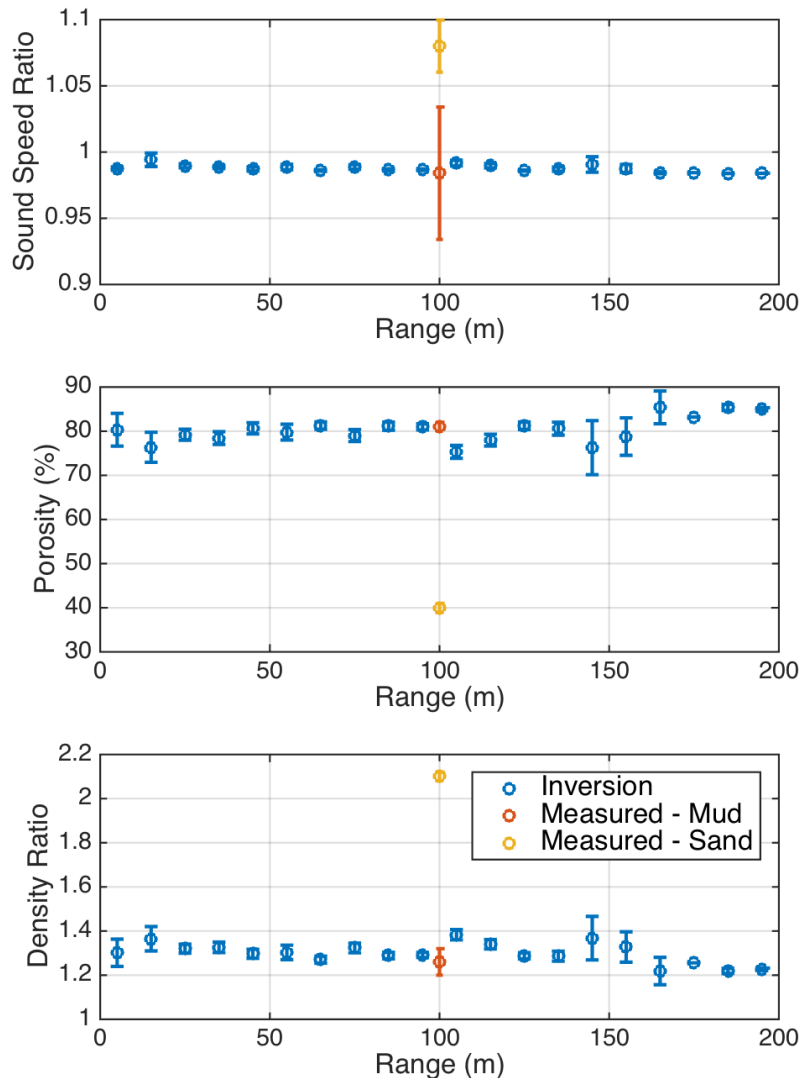


Figure 36: Sound Speed Ratio (upper), Porosity (middle), and Density Ratio (lower) for BayEx14 determined using the *IOI* determined from the inversion. The measured values are also shown.

complexity of the environment. The inversion treats this layered medium as a half-space, with no layer, and, as a result, is ignoring the mud layer. Treating the medium as a half-space, it assumes that the sand/mud boundary is abrupt and also ignores the transition layer that is clearly visible in the conductivity probe data. This leads to low values for the reflection coefficient and hence the *IOI* produced at this transition. While it fails to account for this smooth transition, it does seem to treat the variation in depth of the sand/mud interface as volume scattering.

This complexity could be captured by the inversion by introducing more free parameters into the first stage of processing as seen in Figure 33. The mud layer could be accounted for by allowing the possibility of a layer by introducing depth-dependent volume scattering and/or additional 2D distributions of point interface scatterers at arbitrary depths. This would greatly increase the number of parameters that the inversion would need to search over both increasing the computation time and the uncertainties in the output. Ignoring these difficulties for the moment, suppose that the inversion works and it correctly identifies aspects of the sediment such as the mud layer and the transition layer from the mud into the sand. For the applications that are of interest to SERDP, these outputs would need to be used as inputs to models such as PC SWAT or into target scattering models. These models, however, are not currently designed to handle this level of complexity and as result would fail to correctly capture the acoustic response of the environment. It is reasonable to conclude that the complexity of the inversion algorithm should reflect the complexity of the models that rely on its output.

If the simplicity of the inversion algorithm is maintained even for this complex environment, are the outputs of the inversion correct? The inversion fits the MBES time series so the outputs are those required to produce the best fit of the data for the frequency band and the incident angles used in the inversion. As a result, using these outputs with a code such as PC SWAT should produce the correct reverberation levels under the same conditions. The question remains as to whether the results from PC SWAT would still be correct if it were to model smaller grazing angles or frequencies using the inversion output. To properly address this question would require that the models used to evaluate the inversion performance to account for the complexity of the environment and produce the effective response of the sediment. While there are tools available to extend our scattering models to capture this complexity, due to the difficulty of the problem and amount of time this effort would require, it could not be accomplished as a part of this project.

Anecdotally, there is evidence that the BayEx14 inversion did produce parameters that correctly capture the acoustic response of the medium at lower grazing angles and frequencies. In performing data/model comparisons for the target scattering experiments that took place during BayEx14, Dr. Steve Kargl and Dr. Aubrey Espana have found the best comparisons with the data occur when the sediment density is assumed to be 1.3 g/cm^3 consistent with the results of the inversion [24]. This data is for scattering from targets that are resting on the sand/mud interface and for acoustic signals incident at shallow grazing angles and frequencies less than 30 kHz. The model in this case assumes a half-space and neglects the mud layer.

Conclusions and Implications for Future Research/Implementation

The goal of this project was to develop a high frequency, physics-based sonar inversion and test its performance in a series of field experiments. The first of these experiments, GulfEx11, which took place prior to the start of this project, was hampered by the presence of fish, problems with the environmental measurements, and issues with saturation of the 7125 returns. Despite these issues, the data provided a starting point for the inversion development and the opportunity to learn what was needed and what should be avoided in the next two experiments. These lessons were successfully applied in TREN13 and BayEx14, and data sets were collected of sufficient quality to perform the inversion evaluations that were needed.

For TREN13, the MBES had to be mounted on a pole alongside the ship, which led to instabilities and artifacts in some of the data. As a result, we had to develop a rejection criterion to remove these spurious data points, thus reducing our data coverage of the site. This turned out not to be an issue for a majority of the data products from the inversion since they are frequency independent and can be averaged across the entire frequency band. The exception was the volume scattering strength, which is frequency dependent, and the results were sparse both along track and in frequency. Placing the sonar in the moon well of the vessel during BayEx14 significantly improved the quality and stability of the data and we would expect a similar improvement in data quality for the TREN13 site if the sonar had been placed in the well.

At the TREN13 experiment site, there were two seabed regions covered by the MBES track; A region which was composed sand with a shell and shell hash fraction that increased with range and a region beyond 200 m along the track that was composed of mud and sand in unknown proportions up until 350 m where it changed back to a shell and sand mix. The goal of this field test was to test the inversion using a sand environment and hence the first 200 m were the focus of the environmental characterization. In this region, the roughness power spectrum obtained by inversion compared well with the ground truth measurements and inversion slightly overestimated the values for most of the *IOI* derived quantities. This overestimation is consistent with an increase in the reflection coefficient due to the large quantity of shell hash lying on the seafloor in this region.

The loss parameter was determined during both the first stage of the inversion and from the *IOI* found in the second stage of the inversion. The loss parameter from the second stage compared well with the ground truth measurements while the loss parameter from the first stage was a significantly lower. This indicates that the inverted loss accounts for only the intrinsic attenuation, while the *IOI* loss captures both the intrinsic and scattering losses. The volume scattering strengths determined from the inversion underestimate the model predictions, but this may be a failure of the model to account for the significant levels of multiple scattering that should be expected to occur in this environment. There are also fluctuations in the inverted volume scattering strength along the track that may be due to variations in the environment or instabilities in the sonar mounting. The

relative importance of these two sources of variation cannot be determined using this data set.

The BayEx14 environment was arguably an order of magnitude more complicated than the TREX13 site in that there was a mud layer over a mixed sand mud half-space and a transition layer that had significant depth fluctuations (characterized as roughness in Figure 28). At its current level of sophistication, the inversion treated this environment as a half-space and as a result the outputs were effective values based on this approximation. These effective values did not necessarily reflect the ground truth measurements, but there is reason to believe that these may be the correct parameters to use in a model such as PC SWAT. Due to the complexity of the environment, at this time we can only hypothesize what mechanisms, such as the transition layer and volume scattering at the sand/mud interface, need to be included in the scattering models to perform a proper evaluation of the inversion's performance.

Despite this hurdle to fully evaluating the inversion performance for BayEx14, the inversion has reached a level of maturity with this field test that puts it at the cutting edge of remote seabed characterization particularly for those applications that are of most interest to the UXO detection problem. Taking a physics-based approach insures that the output of the inversion addresses the needs of modeling codes and simulations that incorporate similar physical models. Any inversion becomes unstable as the complexity of its underlying model is increased. This complexity can be constrained by the maintaining the same level of complexity of the scattering and simulation codes that the inversion is being designed to support. Using the half-space model, the inversion was able to be applied seamlessly to both the TREX13 and the BayEx14 MBES data, producing stable results in these complex environments while still providing meaningful outputs.

Focusing on the application of the inversion data products also suggests a more meaningful approach to evaluating the inversion performance:

1. Collect MBES data and invert the data.
2. Collect a second set of acoustic data in the same area using a different sonar (side scan, SAS, etc.).
3. Simulate the second set of acoustic data using the outputs from the inversion and compare that simulation to the measured data.

This approach removes the requirement for ground truth measurements and directly addresses the SERDP needs. A similar approach could be taken to support modeling of UXO burial but it is unclear to the author at this time what inputs are needed to those models and to what level of sophistication those models have evolved.

Our experiences with data collection in these three experiments also indicate that a new data collection approach is needed. In TREX13 and BayEx14, data was collected along the measurement track by driving the boat back and forth and changing the frequency for each pass. This is time-consuming and impractical for a wide area survey. A better

approach would be to change frequencies for each ping during a pass along a single survey track. For those data products that are frequency independent, the data density would not reduce. For the volume scattering strength, the reduction in data density at each frequency may be offset by the improvements in data quality that would come from collecting all of the data in a single pass. Discussions with engineers at Teledyne-RESON indicate that this approach could be implemented with the addition of an external PC control that would avoid modifying the existing suite of software that runs the sonar. This not only simplifies the implementation but also provides a transition path where this capability could be added to existing 7125s. Development of this system would require that we move away from the approach taken in this project where we have borrowed sonars from the Teledyne-RESON and instead purchase a sonar that could be used exclusively in developing and testing the frequency-hopping approach.

Literature Cited

- [1] J. L. Galloway and W. T. Collins, “Dual-frequency acoustic classification of seabed habitat using the QTC VIEW,” presented at the Oceans 98, Nice, France, 1998.
- [2] M. Preston, A. Rosenberger, and W. T. Collins, “Bottom classification in very shallow water,” presented at the ECUA 2000, Lyon, France, 2000, pp. 293–299.
- [3] K. Ellingsen, “Acoustic classification of seabed habitats using the QTC VIEW™ system,” *ICES Journal of Marine Science*, vol. 59, no. 4, pp. 825–835, Aug. 2002.
- [4] R. C. Chivers, N. Emerson, and D. R. Burns, “Seabed classification using the backscattering of normally incident broadband acoustic pulses,” *Hydrographic J.*, vol. 26, pp. 9–16, 1982.
- [5] G. J. Heald, “High frequency seabed scattering and sediment discrimination,” in *Acoustical Oceanography*, vol. 23, Southampton, UK, 2001, pp. 258–267.
- [6] O. Humborstad, K. E. Nøttestad, L. Løkkeborg, and H. T. Rapp, “RoxAnn bottom classification system, sidescan sonar and video-sledge: spatial resolution and their use in assessing trawling impacts,” *ICES Journal of Marine Science*, vol. 61, no. 1, pp. 53–63, Feb. 2004.
- [7] E. Pouliquen and X. Lurton, “Seabed identification using echo-sounder signals,” *ECUA 1992*, pp. 535–538.
- [8] D. D. Sternlicht and C. P. de Moustier, “Time-dependent seafloor acoustic backscatter (10-100 kHz),” *J. Acoust. Soc. Am.*, vol. 114, no. 5, pp. 2709–2725, Nov. 2003.
- [9] D. D. Sternlicht and C. P. de Moustier, “Remote sensing of sediment characteristics by optimized echo-envelope matching,” *J. Acoust. Soc. Am.*, vol. 114, pp. 2727–2743, Nov. 2003.
- [10] C. De and B. Chakraborty, “Acoustic characterization of seafloor sediment employing a hybrid method of neural network architecture and fuzzy algorithm,” *Geoscience and Remote Sensing Letters, IEEE*, vol. 6, no. 4, pp. 743–747, 2009.
- [11] D. R. Jackson and M. D. Richardson, *High-Frequency Seafloor Acoustics*. New York, NY: Springer, 2006.
- [12] K. B. Briggs, D. Tang, and K. L. Williams, “Characterization of interface roughness of rippled sand off Fort Walton Beach, Florida,” *IEEE J. Ocean. Eng.*, vol. 27, no. 3, pp. 505–514, 2002.
- [13] D. Tang, “Fine-scale measurements of sediment roughness and subbottom variability,” *IEEE J. Ocean. Eng.*, vol. 29, pp. 929–939, 2005.
- [14] C.-C. Wang and D. Tang, “Application of Underwater Laser Scanning for Seafloor Shell Fragments Characterization,” *Journal of Marine Science and Technology-Taiwan*, vol. 20, no. 1, pp. 95–102, Feb. 2012.
- [15] W. Chau-Chang and C. Min-Shine, “Nonmetric Camera Calibration for Underwater Laser Scanning System,” *IEEE J. Ocean. Eng.*, vol. 32, no. 2,

- pp. 383–399, 2007.
- [16] E. I. Thorsos, K. L. Williams, N. P. Chotiros, J. T. Christoff, K. W. Commander, C. F. Greenlaw, D. V. Holliday, D. R. Jackson, J. L. Lopes, D. E. McGehee, J. E. Piper, M. D. Richardson, and D. Tang, “An overview of SAX99: acoustic measurements,” *IEEE J. Ocean. Eng.*, vol. 26, no. 1, pp. 4–25, 2001.
- [17] M. J. Buckingham and M. D. Richardson, “On tone-burst measurements of sound speed and attenuation in sandy marine sediments,” *IEEE J. Ocean. Eng.*, vol. 27, no. 3, pp. 429–453, 2002.
- [18] B. T. Hefner, “Inversion of high frequency acoustic data for sediment properties needed for detection and classification of UXOs,” Interim Report for MR-2229, Feb. 2013.
- [19] G. Wendelboe, H. Dahl, E. Maillard, and L. Bjorno, “Towards a fully calibrated multibeam echosounder,” *ECUA 2012 11th European Conference on Underwater Acoustics*, vol. 17, pp. 070025–070025, 2012.
- [20] K. L. Williams, D. R. Jackson, E. I. Thorsos, D. Tang, and K. B. Briggs, “Acoustic backscattering experiments in a well characterized sand sediment: data/model comparisons using sediment fluid and Biot models,” *IEEE J. Ocean. Eng.*, vol. 27, no. 3, pp. 376–387, 2002.
- [21] A. P. Lyons, “The Potential Impact of Shell Fragment Distributions on High-Frequency Seafloor Backscatter,” *IEEE J. Ocean. Eng.*, vol. 30, no. 4, pp. 843–851, Oct. 2005.
- [22] A. N. Ivakin, “Discrete scattering in stratified marine sediments: A modeling approach and application to a shelly sand-mud environment,” *Proc. Tenth European Conference on Underwater Acoustics (ECUA2010)*, Istanbul, Turkey, 2010, vol. 3, pp. 1432–1439.
- [23] A. P. Lyons and T. H. Orsi, “The effect of a layer of varying density on high-frequency reflection, forward loss, and backscatter,” *IEEE J. Ocean. Eng.*, vol. 23, no. 4, pp. 411–422, Oct. 1998.
- [24] S. G. Kargl, Personal Communication, April 20, 2015.